Available online at www.sciencedirect.com

SciVerse ScienceDirect

Proceedings of the Combustion Institute 34 (2013) 1–31

Proceedings of the Combustion Institute

www.elsevier.com/locate/proci

Small scales, many species and the manifold challenges of turbulent combustion

Stephen B. Pope

Sibley School of Mechanical and Aerospace Engineering, Cornell University, Ithaca, NY 14853, USA

Available online 13 October 2012

Abstract

A major goal of combustion research is to develop accurate, tractable, predictive models for the phenomena occurring in combustion devices, which predominantly involve turbulent flows. With the focus on gas-phase, non-premixed flames, recent progress is reviewed, and the significant remaining challenges facing models of turbulent combustion are examined. The principal challenges are posed by the small scales, the many chemical species involved in hydrocarbon combustion, and the coupled processes of reaction and molecular diffusion in a turbulent flow field. These challenges, and how different modeling approaches face them, are examined from the viewpoint of low-dimensional manifolds in the high-dimensional space of chemical species. Most current approaches to modeling turbulent combustion can be categorized as flamelet-like or PDF-like. The former assume or imply that the compositions occurring in turbulent combustion lie on very-low-dimensional manifolds, and that the coupling between turbulent mixing and reaction can be parameterized by at most one or two variables. PDF-like models do not restrict compositions in this way, and they have proved successful in describing more challenging combustion regimes in which there is significant local extinction, or in which the turbulence significantly disrupts flamelet structures. Advances in diagnostics, the design of experiments, computational resources, and direct numerical simulations are all contributing to the continuing development of more accurate and general models of turbulent combustion.

Keywords: Turbulent combustion; Probability density function methods; Large-eddy simulation

1. Introduction

Turbulent combustion, the topic of this paper, has been the focus of previous Hottel lectures [1,2] and of many other plenary lectures [3–10] at the International Combustion Symposia. The topic is both important and persistent. The importance is obvious, given the continuing dominance of the combustion of hydrocarbon fuels to meet the world's energy demands, and the fact that the flows involved are inevitably turbulent, because of their large flow rates. The persistence of research on turbulent combustion over many decades reflects the formidable challenges of the subject, which yield slowly to our increasing understanding and technological capabilities in terms of computer power and instrumentation.

1.1. Turbulent combustion models: goals and lines of attack

As in most branches of the physical sciences, the ultimate goal of research on turbulent combustion is an accurate and tractable theory or model, which encapsulates the attained knowledge

E-mail address: s.b.pope@cornell.edu (S.B. Pope).

1540-7489/$ - see front matter
http://dx.doi.org/10.1016/j.proci.2012.09.009

and understanding of the phenomenon. For example, in the context of ground transportation, a US Department of Energy workshop [11] "identified a single overarching grand challenge: the development of a validated, predictive, multi-scale combustion modeling capability to optimize the design and operation of evolving fuels in advanced engines for transportation applications". While the use and value of turbulent combustion models continue to increase across combustion industries, current capabilities fall well short of what is needed in reliable design tools, and well short of what has been achieved in other disciplines, such as solid mechanics and fluid dynamics.

One line of attack is to develop models applicable to the geometry of practical combustion devices, including sub-models for the many complexities involved—sprays, radiation, acoustics, etc.—in addition to a turbulent combustion model for the gas-phase combustion. For the overall model to be computationally tractable, each sub-model needs to be relatively simple. A marvelous exemplar of this line of attack is the simulation by Boileau et al. [12] of the ignition sequence of the 18 liquid-fueled burners in a gas-turbine annular combustor. As our knowledge and computer power increase, the sub-models can be improved in their scope and accuracy. While this line of attack is extremely valuable, it has to confront two difficulties. First, the quality and quantity of experimental data for model validation in such applications are quite limited. Second, when there are discrepancies between simulations and experimental data, it can be difficult to determine which sub-model (or combination of sub-models) is to blame.

A different, complementary line of attack is, to the extent possible, to separate and isolate the different phenomena involved, and to study them in laboratory experiments in relatively simple geometries. With this approach, much more comprehensive and accurate measurements are possible; the phenomena are more amenable to direct numerical simulation (DNS); and the information from experiments and DNS can be used directly to test sub-models, identify deficiencies, and suggest directions for improvements. This is a surer way to develop fundamentally sound and validated models. However, this line of attack has its own set of issues: it takes a longer time to make an impact on the design of combustion devices; a set of tractable sub-models may be intractable when they are combined; and, the experiments and DNS performed may not be at conditions representative of practical applications. The latter point is a particular concern: while laboratory experiments are generally designed to yield the relevant combustion regime (e.g., as characterized by the Damköhler number), usually the Reynolds number is lower than in applications (typically by an order of magnitude); and laboratory experiments are predominantly at atmospheric pressure, and typically use simple gaseous fuels.

In this paper, we take the latter line of attack and, putting aside the complexities of sprays, radiation, acoustics, instabilities, etc., we focus on the essence of the turbulent combustion problem, namely the coupled processes of reaction and molecular diffusion in a turbulent flow field. Furthermore, we focus on non-premixed turbulent combustion. We take the viewpoint that the underlying physics and chemistry is known in terms of the conservation equations for mass, momentum, energy and chemical species [13]. While our knowledge of the material properties involved in these equations (chemical reaction rates and thermodynamic and transport properties) contains uncertainties, these will decrease with time: and besides, what other starting point is there for a fundamentally-based theory?

We take it, therefore, that the governing equations satisfy our requirement of "accuracy", but they do not satisfy the requirement of "tractability". This is for two obvious reasons. First, the accurate solution of the governing equations requires the resolution of all length scales and time scales of the problem [3], which, for practical combustion devices, will remain computationally prohibitive for many decades to come [14,15]. Second, chemical mechanisms for many hydrocarbon fuels may involve thousands of species [16]. In order to overcome the challenges of small scales and many species, it seems inevitable that any tractable computational approach must include two ingredients: a statistical description of the small scales; and a reduced description of the chemistry in terms of far fewer species (or other variables).

1.2. Progress towards the ultimate goal

Two fundamental questions we can ask are: at some point in the future, when the challenges of modeling turbulent combustion have been completely overcome, what will be the nature of the victorious, ultimate turbulent combustion model? And, how will progress continue to be made towards this goal?

We can get some clues to the answer to the first question by examining a much simpler, now-solved problem, namely the numerical solution of ordinary differential equations (ODEs). There are now completely satisfactory solution methodologies (and software packages) both for initial-value problems and for boundary-value problems (e.g., [17]). In these methods there are just two types of user input: the first is the problem statement (domain, governing equations, material properties, initial or boundary conditions); the second is an error tolerance. The methodology then determines a numerical solution which is

accurate to within the specified error tolerance. An essential ingredient of such methodologies is *adaptivity*, both of the mesh and of the order of finite-difference (or similar) approximation used. And, in order to implement an adaptive strategy, it is necessary to be able to estimate the error incurred using a particular scheme on a particular mesh. For complex problems, adaptivity allows the use of a detailed description of the phenomena in the (usually small) regions where it is necessary, while avoiding the concomitant high cost in the regions where the detailed description is not necessary.

Similarly to the example of the ODEs, in the ultimate turbulent combustion model there will be several types of adaptivity, and there have already been initial steps in this direction including: adaptive mesh refinement (AMR) [18]; adaptive chemistry [19–24]; and adaptive turbulence modeling (e.g., hybrid RANS/LES [25,26]). In some of these aspects of the problem (e.g., AMR and adaptive chemistry) there are established ways to estimate error: in the modeling of turbulence and turbulence-chemistry interactions, estimating errors is much more challenging.

At present, many turbulent combustion models are designed for (and restricted to) particular special cases, such as premixed combustion or non-premixed combustion with two uniform streams (i.e., fuel and oxidant). In contrast, the ultimate combustion model will be generally applicable, even though through adaptivity it may make use of specialized models. Such generality is highly desirable, since practical combustion problems seldom conform to the idealizations used in the specialized models, and they may involve two or more distinct combustion modes or regimes. Furthermore, the ultimate, adaptive turbulent combustion model requires of the user much less knowledge and skill than is currently required to select and apply specialized models.

In addressing the second question—how will progress continue to be made towards the goal of achieving a completely satisfactory model of turbulent combustion?—it is important to recognize that there is a broad range of turbulent combustion problems, ranging in their complexity and challenges. As discussed elsewhere [27], it is therefore valuable to have a range of modeling approaches, from simple models for less challenging problems, to more complex and costly models for more challenging problems. With sustained research effort, we see progress of two kinds. First the frontier of our modeling capabilities advances, in the sense that more complex models are developed to treat some of the previously-unmet challenges. Second, behind this advancing frontier, the models are refined, their accuracy is improved, their range of applicability and accuracy are delineated, error estimators are developed, and improved software becomes more widely available.

1.3. Scope, themes and outline of the paper

To provide the necessary background for the subsequent discussions, in Section 2 we present the conservation equation for chemical species and review some of its basic properties. In Section 3 we consider the principal challenges facing models of turbulent combustion. As mentioned, meeting the challenges of small scales inevitably requires a statistical approach, so that the coupled processes of reaction and molecular diffusion have to be modeled. The present paper focuses on this challenge in the context of non-premixed turbulent combustion.

Based on how they address the challenge posed by the coupling between chemical reactions and molecular diffusion, most current approaches fall into one of two distinct categories, which we refer to as *flamelet-like* and *PDF-like*. These two types of models are discussed in Sections 4 and 5, respectively, and their characteristics are contrasted in Table 2 in Section 7. Section 5 includes a brief account of the successes achieved by PDF methods in the past decade in accurately representing the challenging phenomena of local extinction and ignition. A crucial distinction between the two types of models is that flamelet-like models assume (or imply) that, in the high-dimensional space of species, the compositions that occur in turbulent combustion are confined to very-low-dimensional manifolds.

A theme of the paper is the examination of the processes of reaction and molecular diffusion from the perspective of manifolds in the species space. In Section 6 we classify and examine the various manifolds used in turbulent combustion and discuss the implications of these considerations for models of turbulent combustion. The species conservation equation expressed relative to a low-dimensional manifold reveals the important balance (or imbalance) between reaction and molecular diffusion, with the latter appearing as the product of a scalar dissipation and the curvature of the manifold. Many, if not all, approaches to non-premixed turbulent combustion lead to governing equations with the same structure.

In Section 7, conclusions are drawn and some opinions are given on the future development of turbulent combustion models. While flamelet-like models have a significant and useful role to play, they depend on the very strong assumption that the compositions occurring in turbulent combustion lie on a very-low-dimensional manifold (e.g., 2D or 3D). It is abundantly clear that this assumption is not tenable in some of the more challenging regimes of turbulent combustion. PDF-like approaches avoid the assumption of a very-low-dimensional manifold, and can be expected to continue to advance the frontiers of our capabilities to more challenging combustion regimes.

While most of the paper is in the form of exposition, review and discussion, an original contribution is the analysis in Appendix A which provides a link between PDF-like and flamelet-like models.

2. Species conservation

2.1. Simplified conservation equations

We introduce here a simplified equation for species conservation. This is sufficient for us to study the essence of the turbulent combustion problem and the theories described in later sections.

We consider the low-Mach-number flow of a reactive ideal gas mixture (e.g., a gas-fueled, non-sooting, turbulent flame). The fields of fluid density and velocity are denoted by $\rho(\mathbf{x},t)$ and $\mathbf{U}(\mathbf{x},t)$, and the mass fractions of the n_s chemical species are denoted by $\mathbf{Y}(\mathbf{x},t) = \{Y_1, Y_2, \ldots, Y_{n_s}\}$.

The species conservation equation considered is

$$\frac{DY_i}{Dt} = \frac{1}{\rho}\nabla\cdot(\rho D\nabla Y_i) + S_i, \tag{1}$$

where the material derivative $D/Dt \equiv \partial/\partial t + \mathbf{U}\cdot\nabla$ gives the rate of change following the fluid; D is the molecular diffusivity; and S_i is the net creation rate of species i due to chemical reactions. We refer to $\mathbf{S} = \{S_1, S_2, \ldots, S_{n_s}\}$ as the chemical source term. The only simplification contained in this equation is the use of Fick's law with equal diffusivities for all species. It is well appreciated that differential diffusion can be very important in several combustion phenomena [13,28] but the use of a single diffusivity retains the essence of the problem studied, while affording significant simplifications of the subsequent equations.

At each point in the flow, the thermochemical state of the fluid is fully characterized by the species mass fractions $\mathbf{Y}$, the pressure p, and the enthalpy h. We consider flows such as open laboratory flames in which pressure variations are negligible (compared to the absolute pressure). We also take the enthalpy to be a known linear function of $\mathbf{Y}$, as is the case in idealized premixed and non-premixed flames (with unity Lewis number and negligible heat loss). Thus, the spatial and temporal variation of the thermochemical state is fully described by $\mathbf{Y}(\mathbf{x},t)$. Hence, from the known thermodynamic properties, we have equations of state for density and temperature of the form

$$\rho(\mathbf{x},t) = \hat{\rho}(\mathbf{Y}(\mathbf{x},t)), \text{ and}$$
$$T(\mathbf{x},t) = \widehat{T}(\mathbf{Y}(\mathbf{x},t)), \tag{2}$$

the known transport properties provide the diffusivity

$$D(\mathbf{x},t) = \widehat{D}(\mathbf{Y}(\mathbf{x},t)), \tag{3}$$

and the known chemical kinetics determine the chemical source term

$$\mathbf{S}(\mathbf{x},t) = \widehat{\mathbf{S}}(\mathbf{Y}(\mathbf{x},t)). \tag{4}$$

(The notation distinguishes between quantities expressed as functions of position and time, e.g., $\mathbf{S}(\mathbf{x},t)$, and the same quantity expressed as a function of mass fraction, i.e., $\widehat{\mathbf{S}}(\mathbf{Y})$). The chemical source term can be decomposed into production ($\mathbf{S}^+$) and consumption ($\mathbf{S}^-$) rates

$$\widehat{S}_i = S_i^+ - S_i^- = S_i^+ - Y_i/\tau_{(i)}, \tag{5}$$

where the time scales τ_i are defined by the latter equation, and bracketed subscripts are excluded from the summation convention.

It is emphasized that the assumptions—unity Lewis numbers, constant pressure, enthalpy linear in $\mathbf{Y}$—are made here just to simplify the exposition. In most modeling approaches, some or all of these assumptions are avoided.

For non-premixed combustion involving two uniform streams—a fuel stream of composition $\mathbf{Y}^{\mathrm{fu}}$ and an oxidant stream of composition $\mathbf{Y}^{\mathrm{ox}}$—we introduce the mixture fraction $Z(\mathbf{x},t)$, which is defined to be unity in the fuel stream, zero in the oxidant stream, and to evolve by

$$\frac{DZ}{Dt} = \frac{1}{\rho}\nabla\cdot(\rho D\nabla Z). \tag{6}$$

It follows from the assumptions made that the enthalpy, the mass fractions of the elements, and the mass fractions of inert species are all known linear functions of mixture fraction.

2.2. Basic observations

We now make some basic observations about the species conservation equation, and recall some well known results.

1. Given the complexity of turbulent combustion, it is reassuring to observe from Eq. (1) that, following the fluid, there are only two processes that directly affect the chemical composition, namely, reaction and molecular diffusion.
2. A turbulent velocity field does not directly affect the composition of a fluid particle, in the sense that $\mathbf{U}(\mathbf{x},t)$ does not appear in Eq. (1). It does, however, have a strong indirect effect, primarily through the action of turbulent straining to intensify gradients and hence to increase molecular diffusive fluxes. This may be seen through the equation for species gradients

$$\frac{DY_{i,j}}{Dt} = \nabla\cdot(D\nabla Y_{i,j}) - U_{k,j}Y_{i,k} + J_{ik}Y_{k,j}, \tag{7}$$

where we define $Y_{i,j} \equiv \partial Y_i/\partial x_j$ and $U_{i,j} \equiv \partial U_i/\partial x_j$, and $\mathbf{J}(\mathbf{Y})$ is the Jacobian of the chemical source term

$$J_{ij}(\mathbf{Y}) \equiv \frac{\partial \widehat{S}_i(\mathbf{Y})}{\partial Y_j}. \tag{8}$$

(Eq. (7) follows from Eq. (1) for the simplest case of constant-property flow.) The penultimate term in Eq. (7) shows that compressive straining in the direction of $\nabla\mathbf{Y}$ intensifies species gradients.

3. For inert species and for mixture fraction, as is evident from Eq. (7), straining by the velocity field is the only mechanism for the intensification of species gradients. For reactive species, on the other hand, chemical reactions can also have a significant effect on species gradients (*via* the final term in Eq. (7)).
4. The species conservation equation admits a solution corresponding to a steady, one-dimensional, plane, premixed, laminar flame propagating at the laminar flame speed s_L relative to the unburnt mixture. For a given fuel, pressure and unburnt temperature, let s_L^o denote the laminar flame speed of the stoichiometric mixture, and let D_u denote the diffusivity of the unburnt mixture. From these two quantities we obtain the length scale $\delta_L \equiv D_u/s_L^o$ (a measure of the flame thickness), and the time scale $\tau_c \equiv \delta_L/s_L^o$ which we use henceforth as the characteristic time scale of the overall chemical reaction.
5. In contrast to the premixed case, for non-premixed combustion there are no inherent length and time scales provided by the thermochemical and transport properties alone. These scales arise from the interaction of the flow with the combustion.
6. Perhaps the simplest instance of non-premixed combustion is the steady, laminar, counter-flow flame that occurs between opposed jets of fuel and oxidant [28,29]. Along the centerline (taken to be the x_1 axis), to a good approximation, the composition field is one-dimensional (i.e., $\mathbf{Y}(x_1)$), and the mixture fraction $Z(x_1)$ varies monotonically with x_1, from zero in the oxidant jet to unity in the fuel jet. Consequently, species mass fractions can be viewed as single-valued functions of mixture fraction, i.e., $\mathbf{Y}(x_1) = \mathbf{Y}^{\rm cf}(Z(x_1))$. By substituting this relation into Eq. (1), we deduce that this functional dependence is determined as the solution to the ordinary differential equation:

$$0 = \frac{1}{2}\chi\frac{d^2\mathbf{Y}^{\rm cf}}{dz^2} + \widehat{\mathbf{S}}(\mathbf{Y}^{\rm cf}(z)), \tag{9}$$

where z is an independent mixture-fraction variable, and χ is the all-important scalar dissipation

$$\chi \equiv 2D|\nabla Z|^2, \tag{10}$$

which has dimensions of inverse time.

This is the first of several equations we shall encounter showing the balance (or imbalance) between reaction and molecular diffusion, the latter appearing as the product of a scalar dissipation and the curvature of a manifold (here $d^2\mathbf{Y}^{\rm cf}/dz^2$). (Here and below, somewhat loosely, we refer to the second derivative of the manifold as "curvature", since it is indeed the curvature of the manifold which is the significant quantity.)

3. The challenges of modeling turbulent combustion

We outline here the principal challenges that have to be faced in the modeling of turbulent combustion; that is, the obstacles that have to be overcome in order to construct an accurate, tractable model based on the species conservation equation, Eq. (1). Depending on how they address these challenges, most current models can be classified as either flamelet-like or PDF-like. The characteristics of these two classes of models are described in Section 3.2.

3.1. The principal challenges

3.1.1. Many species

For hydrocarbon combustion there may be 50–7000 species involved, depending on the fuel [16]. However, for many fuels, chemical mechanisms are available which contain 150–250 species [30]. Clearly, it is highly beneficial, usually essential, to reduce the number of species that have to be considered. Some of the available dimension reduction techniques are discussed in Section 6. Important conclusions from research in the last two decades (e.g., [31,32]) are that, for simple hydrocarbon fuels, accurate descriptions over a range of conditions are possible with of order 20–40 species, but certainly not with of order five species.

3.1.2. Small scales

In order to solve numerically the species conservation equation (Eq. (1)), it is necessary to resolve all length and time scales. The length scales vary from the size of the device or apparatus down to the smallest scales, which may be the Kolmogorov length scale of turbulence, or, in some combustion regimes, the yet smaller scales occurring in reaction zones (e.g., δ_L). The relevant time scales are from the residence time down to the smaller of the Kolmogorov timescale, τ_η, and the smallest chemical time scale, which may be of order 10^{-10} s, or even smaller (depending on the fuel and conditions).

Because of this very large range of scales, it is well-appreciated that DNS of combustion devices will remain infeasible for many decades to come [33]. It is inevitable that a tractable modeling approach treats the small-scale processes statistically, rather than resolving them. Hence, the

tractable approaches that have been developed are in the context of either RANS or LES. In RANS (Reynolds-averaged Navier–Stokes) all scales are treated statistically; whereas in LES (large-eddy simulation) the large scales are resolved, and only the small scales are treated statistically [14].

3.1.3. Non-linear chemical kinetics and large turbulent fluctuations

The combination of these two separate characteristics of turbulent combustion dooms simple moment models.

In turbulent flows, fluctuations are typically of order 25%, corresponding to temperature fluctuations of several hundred Kelvin in a typical flame (see, e.g., [34]). Arrhenius chemical reaction rates are highly non-linear functions of temperature. As a consequence of these two facts, there is no hope of an accurate statistical closure based on an expansion about mean properties [15].

Instead, most models (in both RANS and LES) provide some description of the statistical distribution of the fluid composition, most completely through the joint probability density function (PDF) of the species mass fractions and enthalpy. In *assumed PDF* methods, some of which are described in Section 4, the shape of the PDF is prescribed so that the assumed PDF is determined by a few moments (usually means and variances). In *transported PDF* methods (see [35–37] and Section 5), a modeled conservation equation is solved to determine the joint PDF. (Henceforth we refer to transported PDF methods simply as *PDF methods*.)

3.1.4. Large property variations

In atmospheric-pressure flames, the density typically decreases by a factor of 7 between unburnt and burnt fluid; and the kinematic viscosity and diffusivity, D, typically increases by a factor of 20 (see e.g., [38]), while the product ρD typically increases by a factor of 3. The effects of heat release (leading to volume expansion and decreased density) are particularly strong in premixed combustion and can lead to hydrodynamic instabilities and additional mechanisms for turbulence generation, as well as to buoyancy effects.

The strong increase with temperature of the viscosity and diffusivity leads to a significant diminution of the local Reynolds number. The mixture fraction field in a jet flame of jet Reynolds number 15,000 appears very different from that in an inert jet at the same Reynolds number [39].

3.1.5. Coupling between reaction and molecular diffusion

Since molecular mixing occurs dominantly at the smallest scales, its effects have to be modeled in both RANS and LES. For modeling approaches involving variances and covariances, the primary quantities to be modeled are the mean of the scalar dissipation, χ, (of mixture fraction, Eq. (10)) or the mean of the species dissipation tensor

$$\chi_{ij} \equiv D\nabla Y_i \cdot \nabla Y_j. \tag{11}$$

In PDF methods [35], the quantity to be modeled is the *conditional diffusion* defined by

$$G_i(\widehat{\mathbf{Y}},\mathbf{x},t) \equiv \left\langle \frac{1}{\rho}\nabla\cdot(\rho D\nabla Y_i)|\mathbf{Y}(\mathbf{x},t)=\widehat{\mathbf{Y}}\right\rangle, \tag{12}$$

where $\widehat{\mathbf{Y}}$ are independent, sample-space variables corresponding to $\mathbf{Y}$ (angled brackets denote means, and $\langle a|b\rangle$ denotes the mean of a conditional on b).

We distinguish between *inert mixing* (i.e., the molecular mixing of conserved quantities such as mixture fraction and inert species) and *reactive mixing* (i.e., the molecular mixing of reactive species).

In the case of inert mixing, as mentioned in Section 2.2, the process leading to the smallest scales in the conserved scalar field is the straining of the fluid by the turbulence, which tends to steepen gradients [40]. At high Reynolds number, the process of scale reduction through the turbulent cascade is the rate-limiting process, so that the mean scalar dissipation scales with the inverse of the turbulent integral time scale, independent of the value of the molecular diffusivity. While current models are not perfect, at least in the RANS context, the modeling of inert mixing is broadly satisfactory, and does not constitute a major obstacle.

In the case of reactive mixing, there is an additional process, namely reaction, which can steepen scalar gradients. As is clear from Eq. (7), the relative effectiveness of turbulent straining and reaction in steepening gradients depends on the relative magnitudes of the respective timescales, namely the Kolmogorov time scale τ_η and the chemical time scale τ_c. Their ratio is defined to be the Karlovitz number, $\mathrm{Ka} \equiv \tau_c/\tau_\eta$. For $\mathrm{Ka} \gg 1$, reaction does not significantly affect gradients, and mixing occurs by the same turbulent cascade process as in inert mixing. On the other hand, $\mathrm{Ka} \ll 1$ corresponds to flamelet combustion, in which the dominant balance in Eqs. (1) and (7) is between reaction and diffusion, so that the resulting flamelet structure can be exploited in modeling, as is described in Section 4.

The most significant modeling challenge arises when the Karlovitz number is of order unity, so that both turbulent straining and reaction affect molecular mixing. For then neither the cascade nor the flamelet paradigm is sufficient to determine the small-scale structure, and the rate of mixing is affected by interactions between

reaction, diffusion and turbulent straining on the unresolved, small scales.

It should be recognized that a particular instance of turbulent combustion may span a range of Karlovitz numbers. There may be significant spatial variations of the Kolmogorov scales, and different species can have very different characteristic reaction time scales, and these vary significantly with temperature. For example, there may be a flamelet-like reaction zone (with $\mathrm{Ka} < 1$), with pre-flame mixing and post-flame pollutant reactions occurring at high Karlovitz number. Consequently, there is great value in having a general model, applicable over the full range of Karlovitz numbers.

These issues are discussed further in Section 5.4.

While the focus here is on non-premixed combustion, it should be mentioned that, for premixed combustion, the coupling of reaction and diffusion can lead to thermo-diffusive instabilities [41], which pose another serious modeling challenge, even for $\mathrm{Ka} \ll 1$.

3.2. A classification of models

Over the past decades, there has been a plethora of approaches proposed for modeling non-premixed turbulent combustion, many of which are described in [15,42]. These models generally share the same approaches to deal with the challenges of small scales and many species, namely the use of RANS or LES, and the use of some form of reduced description of hydrocarbon chemistry. But there are diverse approaches taken to describe the coupling between reaction and molecular diffusion. Most, but not all, of these approaches fall into one of two categories, which we refer to as *flamelet-like* and *PDF-like*.

The steady flamelet model (discussed in Section 4.2) is the archetype of flamelet-like models. Their essential characteristics are:

1. Strong assumptions are made about the coupling of reaction and molecular diffusion, implying that the species mass fractions are confined to a very-low-dimensional manifold (e.g., 2D or 3D) in the species space.
2. The properties of the very-low-dimensional manifold are determined by laminar-flame (or similar) calculations prior to the turbulent combustion calculation; and the complexities of the combustion chemistry have to be faced only in these relatively simple calculations.
3. The properties of these manifolds needed in the turbulent combustion calculation are tabulated (which is feasible only for very-low-dimensional manifolds).
4. In the turbulent combustion calculation, it is solely (or primarily) inert mixing that has to be modeled.

Flamelet-like models and associated methods include: the steady flamelet model (SFM) [43,44]; the flamelet/progress variable model (FPV) [45–47]; flame-generated manifolds (FGM) [48]; flame prolongation of ILDM (FPI) [49]; and reaction-diffusion manifolds (REDIM) [50,51]. In the past decade, there has been a resurgence in the use of flamelet-like models, especially in LES. Unsteady flamelet models (UFM) [52,53,44] have all of the flamelet-like characteristics, except that they do not necessarily imply a very-low-dimensional manifold.

PDF methods (discussed in Section 5) are of course the archetype of PDF-like approaches. Their characteristics are:

1. No assumption is made restricting the species to a low-dimensional manifold (beyond assumptions made in reducing the description of the chemistry).
2. In computational implementations, the composition of the fluid is represented by the species mass fractions $\mathbf{Y}^*$ of a large number of particles (or other computational elements).
3. Chemical reactions are treated exactly, without modeling assumptions, through $d\mathbf{Y}^*/dt = \widehat{\mathbf{S}}(\mathbf{Y}^*)$.
4. It is necessary to model the reactive mixing of the species mass fractions.

Compared to flamelet-like models, PDF-like models have the advantages of not restricting compositions to a very-low-dimensional manifold, and of treating reaction exactly. On the other hand, they have to confront the modeling of reactive mixing, and the computational challenge of treating the complexities of combustion chemistry within the turbulent combustion calculation (as opposed to in pre-processing).

In addition to PDF methods, PDF-like models include: multiple mapping conditioning (MMC) [54,55]; the linear-eddy model (LEM) [56,57]; and the one-dimensional turbulence (ODT) model [58,59].

The two classes of models—flamelet-like and PDF-like—are considered in more detail in the next two sections. Their characteristics are contrasted in Table 2 in Section 7.

Not all models fall neatly into either one of these categories. The prime examples (beyond UFM) are the conditional moment closure (CMC) [60–62], and the eddy dissipation concept model (EDC) [63].

4. Flamelet-like models

Perhaps the simplest turbulent flame is the non-premixed flame formed when a hydrogen jet issues into ambient air. Taken from the classic

1948 paper by Hawthorne et al. [64], Fig. 1 shows the measured height of such a flame as a function of the jet velocity. The very clear result, that the flame height is essentially independent of the jet velocity, is very revealing and at first sight puzzling.

The most relevant non-dimensional parameters are the Damköhler number $\mathrm{Da} \equiv \tau_f/\tau_c = d/(U_J\tau_c)$ and the Reynolds number $\mathrm{Re} \equiv U_J d/\nu$, where U_J is the jet velocity, d is the jet nozzle diameter, ν is the kinematic viscosity of the fuel, $\tau_f \equiv d/U_J$ is the flow time scale, and τ_c is the chemical time scale defined in Section 2. As the jet velocity increases, the flow time scale and the Damköhler number decrease and the Reynolds number increases. That the flame height does not vary with Da implies that the chemical reactions are not rate limiting; and that the flame height does not vary with Re implies that molecular diffusion ($D \approx \nu$) is also not rate limiting. We recall that reaction and mixing are the only two processes that directly affect chemical species, and yet neither is rate limiting. It has long been understood that the resolution to this superficial puzzle is that the rate-limiting process is turbulent mixing: the stretching and folding of the fluid by the turbulent velocity field continuously decreases the length scale of the species fields until molecular diffusion—however small—becomes effective. The time scale of turbulent mixing τ_m scales as d/U_J, and so the ratio τ_m/τ_f does not change as the jet velocity increases, hence explaining the constant height of the flame.

This picture amounts to the *mixing-controlled paradigm*, the first of five paradigms of non-premixed turbulent combustion identified by Bilger et al. [5]. It leads to the *equilibrium model* of turbulent combustion, developed in the 1970s, mainly by Bilger and co-workers [65,66]. We briefly describe this model, to illustrate how it overcomes the challenges of small scales and many species, and how it involves a simple low-dimensional manifold in the species space.

4.1. Chemical equilibrium

For hydrogen jet flames, typically the Damköhler number is large, and, locally, the chemical composition is close to chemical equilibrium. The equilibrium composition is determined by the pressure, enthalpy, and element mass fractions, all of which are known in terms of the mixture fraction, and so we denote this equilibrium composition by $\mathbf{Y}^{\mathrm{eq}}(z)$. Thus, the assumption that the fluid in the flame is locally in chemical equilibrium is expressed as:

$$\mathbf{Y}(\mathbf{x},t) = \mathbf{Y}^{\mathrm{eq}}(Z(\mathbf{x},t)). \tag{13}$$

A basic objective of turbulent combustion models is to determine the spatial fields of mean quantities, e.g., the mean density and temperature, $\langle\rho(\mathbf{x},t)\rangle$ and $\langle T(\mathbf{x},t)\rangle$. For species, it is usual to consider density-weighted means (or Favre averages), $\widetilde{\mathbf{Y}} \equiv \langle\rho\mathbf{Y}\rangle/\langle\rho\rangle$. Given the equilibrium assumption (Eq. (13)), all of these means can be determined from the PDF of mixture fraction $\tilde{f}_Z(z;\mathbf{x},t)$. In full, $\tilde{f}_Z(z;\mathbf{x},t)$ is the one-point, one-time, density-weighted probability density function of $Z(\mathbf{x},t)$, i.e., the probability density of the event $\{Z(\mathbf{x},t) = z\}$. Specifically, we have

$$\widetilde{\mathbf{Y}}(\mathbf{x},t) = \int_0^1 \mathbf{Y}^{\mathrm{eq}}(z)\tilde{f}_Z(z;\mathbf{x},t)\,\mathrm{d}z. \tag{14}$$

Consistent with the notion that inert mixing is controlled by the larger turbulent motions, it is found that, at high Reynolds number, the PDF $\tilde{f}_Z$ shows little dependence on Reynolds number [67–69]. In the standard *assumed PDF approach*, the PDF $\tilde{f}_Z$ is assumed to be a beta-function distribution, determined by the mean $\widetilde{Z}$ and variance $\widetilde{Z''^2}$ for which turbulence model equations are solved. Thus the means $\widetilde{\mathbf{Y}}$ are functions of $\widetilde{Z}$ and $\widetilde{Z''^2}$, determined by Eq. (14) and the assumed beta PDF, i.e.,

$$\widetilde{\mathbf{Y}}(\mathbf{x},t) = \widehat{\mathbf{Y}}(\widetilde{Z}(\mathbf{x},t), \widetilde{Z''^2}(\mathbf{x},t)). \tag{15}$$

In practice, in a pre-simulation stage, this function $\widehat{\mathbf{Y}}$ is evaluated and tabulated for use on the turbulent combustion computation.

Although it is not a flamelet model, this basic equilibrium model possesses the characteristics of flamelet-like models, namely:

1. The smallest scales do not need to be represented, because the diffusive processes (for the non-reactive mixture fraction) are controlled by the larger-scale turbulent motions.
2. The many species do not need to be represented in the turbulent combustion model calculation, only the mean and variance of the single mixture fraction.
3. By assumption (Eq. (13)), in the n_s-dimensional species space, all compositions lie on the one-dimensional manifold $\mathbf{Y} = \mathbf{Y}^{\mathrm{eq}}(z)$.

An interesting and revealing result (due to Bilger [66]) is obtained by substituting Eq. (13) into

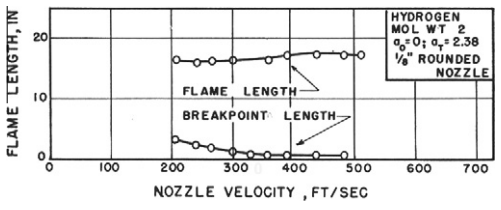

Fig. 1. Flame length of a non-premixed hydrogen flame in air as a function of the nozzle velocity. From [64] with permission of the Combustion Institute.

Eq. (1). After manipulation, but without further assumption, one obtains

$$0 = \frac{1}{2}\chi\frac{\mathrm{d}^2\mathbf{Y}^{\mathrm{eq}}}{\mathrm{d}z^2} + \mathbf{S}, \tag{16}$$

where χ is the scalar dissipation (Eq. (10)). Consistent with the high-Damköhler-number, mixing-controlled paradigm, this equation shows that the creation rate $\mathbf{S}$ of the species is determined, not by the chemical kinetics, but by the mixing rate (characterized by χ) and by the curvature of the manifold.

Eq. (16) appears almost identical to Eq. (9), and indeed both represent a reaction-diffusion balance of the same form. Note, however, that in Eq. (16), $\mathbf{Y}^{\mathrm{eq}}$ is known, and the equation determines $\mathbf{S}$. Conversely, in Eq. (9), $\mathbf{S}$ is a known function, and the equation determines $\mathbf{Y}^{\mathrm{cf}}$.

Our three-dimensional world limits our ability to show manifolds in high-dimensional species spaces: we can visualize them only when they are projected onto two or three-dimensional subspaces. For a particular non-premixed H_2/N_2-air flame, Fig. 2 shows the equilibrium manifold $\mathbf{Y} = \mathbf{Y}^{\mathrm{eq}}(z)$ projected onto the N_2–H_2O–OH mass fraction space. As may be seen, around stoichiometric, there is significant curvature.

The applicability of the chemical-equilibrium model is restricted to very high Damköhler number. While it provides a good model for typical hydrogen flames, for the Damköhler numbers encountered in practice, it is found not to be a good model for hydrocarbon flames.

4.2. Steady flamelet model

The steady flamelet model (SFM) [43] is well known, and considered here only briefly. For fuller discussions see, e.g., [15,44,70].

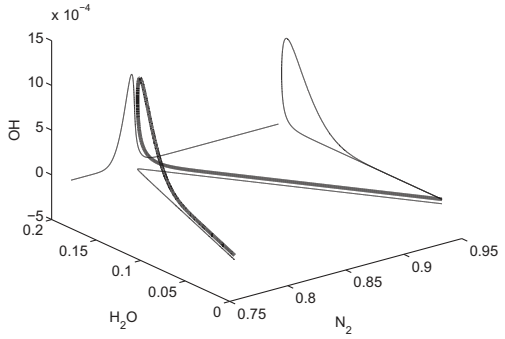

Fig. 2. The equilibrium manifold for a non-premixed H_2/N_2-air flame projected onto the N_2–H_2O–OH mass fraction space (bold line); and projected onto the spaces of N_2–H_2O, N_2–OH, and H_2O–OH (lines, shifted for clarity). The fuel is H_2:N_2, 1:1 by volume, the pressure is 1 bar, and the stream temperatures are 300K. The peak of Y_{OH} on the manifold occurs close to stoichiometric.

The simplest idea leading to the steady flamelet model is that combustion occurs in flamelets (which are thin compared to turbulent scales), whose properties are the same as those of steady, laminar, one-dimensional, counterflow flames. For given compositions of the fuel and oxidant streams, there is a one-parameter family of such counterflow flames, depending on the imposed strain rate. The properties of these flames can be determined from the solution of Eq. (9) together with the mass and momentum equations. For a given imposed strain rate, the resulting scalar dissipation that occurs at the stoichiometric mixture fraction is denoted by χ_{st}, and this is a preferable quantity to use to parameterize the flamelet. Thus, the family of flamelet solutions can be written as $\mathbf{Y}^{\mathrm{sfm}}(z,\chi_{\mathrm{st}})$.

In a turbulent flame, in order to determine the mean composition $\widetilde{\mathbf{Y}}(\mathbf{x},t)$ from the flamelet model, it is necessary to know the joint PDF of Z and χ_{st}. Typically, these two quantities are assumed to be independent; as before, a beta-function distribution is assumed for Z; and a delta-function or log-normal is assumed for χ_{st}.

With respect to the principal issues addressed in the present paper, the steady flamelet model is similar to the equilibrium model:

1. By assumption, in the n_s-dimensional species space, all compositions lie on the two-dimensional manifold $\mathbf{Y} = \mathbf{Y}^{\mathrm{sfm}}(z,\chi_{\mathrm{st}})$.
2. The many species do not need to be represented in the turbulent combustion model calculation, only the mixture fraction (and its dissipation rate).

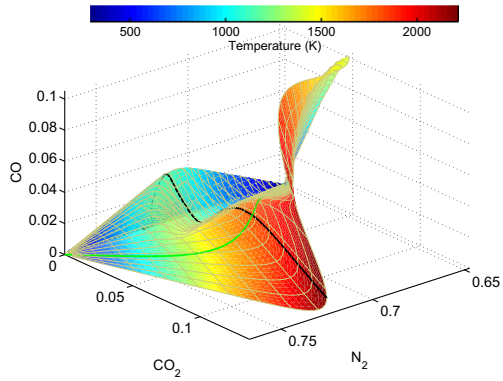

Fig. 3. Steady flamelet manifold projected onto the N_2–CO_2–CO mass fraction space, color-coded by temperature. The oxidant is air; the fuel is methane/air 1:3 by volume (the fuel used in the Barlow and Frank [34] flames); the pressure is 1 bar; and the temperature of both streams is 300K. The green curve corresponds to extinction conditions; the black curve to stoichiometric mixture. The part of the manifold on the near side of the extinction curve (with larger values of CO_2) corresponds to stable flames (from M. Ihme, private communication).

3. The smallest scales do not need to be represented, because the diffusive processes (for the non-reactive mixture fraction) are controlled by the larger-scale turbulent motions.

Fig. 3 shows a steady flamelet manifold $\mathbf{Y} = \mathbf{Y}^{\mathrm{sfm}}(z,\chi_{\mathrm{st}})$ projected onto the N_2–CO_2–CO mass fraction space. The green curve corresponds to the extinction conditions, and in fact only the part of the manifold on the near side of this curve (with larger values of CO_2) is used in the steady flamelet model. Significant curvature of the manifold is evident.

The steady flamelet model is restricted to large Damköhler number such that local extinction of the flamelets does not occur. Several extensions have been proposed, including taking some account of unsteady effects (see, e.g., [70,71]), flame curvature [1], radiative heat transfer [72] and to three feed streams [73].

Compared to the steady flamelet model, there are two significant differences in the flamelet/progress variable model (FPV) [45–47]. First, the whole of the flamelet manifold is used, including the part corresponding to unstable flames. Second, a reaction progress variable $C(\mathbf{x},t)$ is used as the second variable (in place of χ_{st}).

4.3. Strengths and weaknesses of flamelet-like models

Essential characteristics of the flamelet-like turbulent combustion models described above are:

1. By assumption, the compositions that are deemed to occur are confined to a low-dimensional manifold in the species space (generally 2D, sometimes 3D).
2. The thermochemical properties on the manifold are pre-computed and tabulated based on a detailed description of the chemistry.
3. A particular functional form is assumed for the joint PDF of the properties used to parameterize the manifold.
4. Only inert mixing has to be modeled.

From a computational viewpoint, these methods are very attractive because the complexities of the chemistry have to be faced only in the relatively simple task of constructing the manifold. The turbulence modeling task is also relatively simple, since it is the mixing only of the conserved mixture fraction which needs to be represented; and this process is controlled by the larger scales (even though it is effected by the small scales). However, the assumptions made are very strong: that the compositions lie on a low-dimensional manifold, and that the coupling between reaction and mixing in the turbulent flow can be simply parameterized, e.g., by the scalar dissipation. As a consequence, the class of flows for which these assumptions apply is quite limited.

5. PDF-like models

5.1. PDF methods

The characteristics, strengths and weaknesses of PDF methods are quite different from those of flamelet-like models discussed above. Full description of PDF methods can be found in several books and review articles, e.g., [14,35–37,74,75]. Briefly, a modeled conservation equation is solved for the joint PDF of fluid properties, including the species mass fractions and enthalpy. For example, in order to study local extinction and reignition in the Barlow and Frank piloted jet flames [34], Cao and Pope [76] solved for the joint PDF of velocity, turbulent frequency, enthalpy and mass fractions of the 53 species in the GRI3.0 methane mechanism [77].

In contrast to those of flamelet-like models, some characteristics of PDF methods are:

1. The compositions that occur in PDF calculations are not constrained to lie on a low-dimensional manifold (except as may be implied by a reduced-dimension description of the chemistry used).
2. A detailed description of the chemistry (e.g., of order 20–50 species) is used within the turbulent combustion computation (as opposed to being confined to a pre-processing stage).
3. The joint PDF is calculated, based on the modeled conservation equation in which reactive mixing is treated by a *mixing model*.

Simpler turbulent combustion models often depend on non-general concepts, such as mixture fraction and reaction progress variable, and their complexity and cost increases steeply when other effects such as heat loss are included. In contrast, an attractive benefit of PDF methods is that they can readily be applied to more general problems, with multiple streams, partial premixing, stratification, heat loss, etc. Since they provide a complete statistical representation of the thermochemical state, PDF methods also provide an ideal basis for describing other phenomena such as turbulence/radiation interactions [78].

From the computational viewpoint, PDF methods are obviously more demanding, especially because of the inclusion of detailed chemistry. However, several different computational approaches have been developed to make PDF calculations tractable in both RANS and LES [35,79–83]. Prevalent among these is the Lagrangian particle/mesh method [35], in which the distribution of fluid properties is represented by a large

number of particles, each with its own position $\mathbf{X}^*(t)$, species mass fractions $\mathbf{Y}^*(t)$, and other properties depending on the variant used. The properties of these computational particles evolve in time such that their PDF evolves according to the modeled PDF transport equation. In the computational time step Δt, the particle species mass fractions $\mathbf{Y}^*(t)$ evolve due to reaction and molecular diffusion, which are treated in separate fractional steps. In the reaction fractional step $\mathbf{Y}^*(t)$ evolves by $d\mathbf{Y}^*/dt = \widehat{\mathbf{S}}(\mathbf{Y}^*)$—without any modeling assumptions or approximations—and this ability to treat reaction directly and exactly is one of the major virtues of PDF methods. In the mixing fractional step, molecular diffusion is modeled by a *mixing model*. An issue here is that simple mixing models do not account directly for the effects that reaction can have (in some combustion regimes), to steepen gradients, and hence to influence mixing. However, as discussed in Section 5.4, more advanced models can to some extent account for these effects.

In the RANS context, the PDF considered is unambiguously defined as the one-point, one-time, density-weighted, joint PDF of the fluid properties considered. In the LES context there are different possibilities: the interpretation of the PDF as the PDF of fluid properties conditional on the resolved LES fields [74,84] has conceptual advantages over the earlier filtered density function (FDF) [8,75].

In the next two subsections we review two of the successes enjoyed by PDF methods in the past decade in treating some more challenging aspects of non-premixed turbulent combustion.

5.2. Piloted jet flames

For the development of turbulent combustion models, it is essential to have good-quality, detailed experimental data in well-characterized flames designed to explore challenging regimes and phenomena. The paragon of such experiments is the Barlow and Frank study [34] of piloted non-premixed jet flames. The Sydney burner used, developed by Starner and Bilger [85] and investigated by Masri and Bilger [86], is designed to separate extinction from stabilization, so that local extinction can be studied in stable flames.

Out of the series of flames studied by Barlow and Frank [34], most attention has been focused on flames D, E and F in which the fuel-jet bulk velocities are approximately 50 m/s, 75 m/s and 100 m/s, respectively, and the annular pilot jet's velocity is maintained in a fixed proportion. As the jet velocity is increased, the Reynolds number increases, and, more significantly, the Damköhler number decreases. With decreasing Damköhler number, increasing local extinction is observed, with flame F being quite close to global extinction.

The left part of Fig. 4 illustrates the experimental evidence for local extinction. This is a scatter plot of the mass fraction of CO versus mixture fraction obtained in flame F at the axial location where there is most local extinction. Each point in the scatter plot corresponds to a Raman measurement from a single laser shot. The upper curve corresponds to the flamelet profile obtained from the calculation of a mildly-strained laminar flame. Far downstream (not shown), where reignition has occurred, the scatter lies close to this flamelet line, with small conditional fluctuations. But it is evident from Fig. 4 that, at the location shown, the scatter is predominantly below the laminar-flame line (except at small mixture fraction); and, for a given value of mixture fraction, there is considerable scatter in Y_{CO}.

Shortly after the publication of the Barlow and Frank data, there were several PDF studies of these flames [87–89]. The right part of Fig. 4 shows the corresponding scatter plot from the PDF calculation of Xu and Pope [87]. In this case, each point corresponds to the composition of a particle in the particle/mesh method used to solve the PDF equation. As may be seen, the pattern of the scatter is very similar to that of the experimental data, and there is good agreement for the conditional mean of Y_{CO}, which is shown by the lower curves. These PDF calculations are based on the joint PDF of velocity, species mass fractions, enthalpy, and turbulent frequency [14,87]. Important sub-models are the EMST mixing model [90] (which is discussed below in Section 5.4) and a 16-species augmented reduced mechanism (ARM) [31] for methane combustion.

Subsequent investigations [76,91] examined the sensitivity of the PDF calculations to uncertainties in the boundary conditions (mainly the pilot temperature) and to the sub-models. These confirm that (for H–C–O species) the 16-species augmented reduced mechanism yields comparable accuracy to the 53-species GRI3.0 mechanism [77]; and that the EMST model is superior to simpler models.

The amount of local extinction in these flames can be quantified by burning indices. For CO, for example, the burning index BI(CO) is defined as the conditional mean of Y_{CO} within a specified mixture-fraction band around the peak of the laminar flame profile, divided by the peak value of Y_{CO} in the laminar-flame profile. Fig. 4 shows (by vertical dashed lines) the mixture fraction band used, the conditional means (lower symbols), and the peak laminar-flame values (upper symbols). Burning index values of 0 and 1 correspond to complete extinction ($Y_{CO} = 0$) and to complete burning (as in a laminar flame), respectively.

The burning indices for both CO_2 and CO are shown in Fig. 5 as functions of the axial distance. As may be seen, the PDF calculations accurately

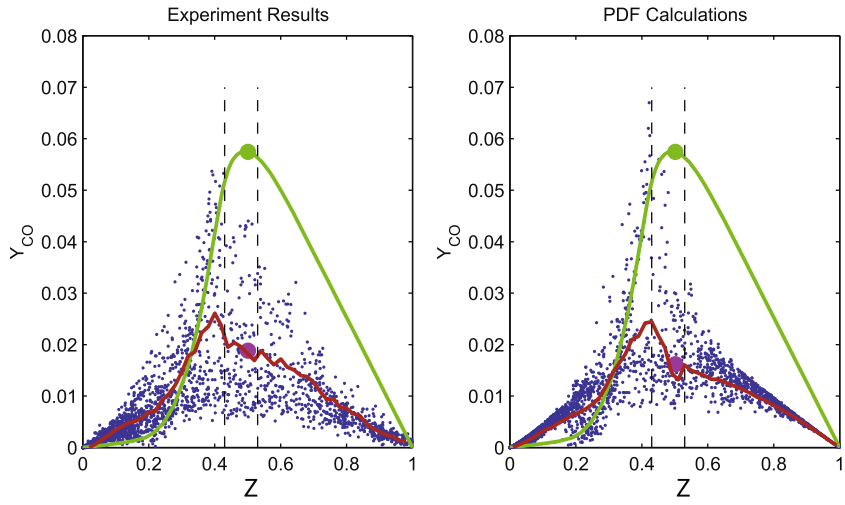

Fig. 4. Scatter plots of the mass fraction of CO versus mixture fraction in flame F at an axial location of 15 jet diameters: left, experimental data [34]; right, PDF calculations [87]. Upper curves, from laminar flame calculations with an imposed strain rate of $a = 100\ s^{-1}$. Lower curves, mean of Y_{CO} conditional on mixture fraction. Vertical dashed lines, specified range of mixture fraction around the peak of the laminar flame profile (upper symbol) used to define the burning index. Lower symbols: conditional mean within the specified mixture fraction range.

describe the level of local extinction in all three flames, as well as the subsequent reignition, leading to the burning indices approaching unity downstream. In the past decade, while there have been many modeling studies of flame D (which exhibits little local extinction), there have been far fewer of flames E and F; and no other approach has demonstrated the ability to represent local extinction and reignition over the full range of conditions and locations that is depicted in Fig. 5.

5.3. Lifted flames in vitiated co-flows

We mention briefly one other flame that demonstrates PDF methods' capabilities of treating the interactions between turbulence and finite-rate chemistry. This is the lifted H_2/N_2 jet flame in a vitiated co-flow studied experimentally by Cabra et al. [92]. Several PDF studies of this flame have been performed [92–97], and it has been studied using LES [98,99], and other approaches [71,100,101]. There have also been DNS studies of similar flames [102].

Early PDF studies revealed that the lift-off height H of the flame is very sensitive to the temperature T_c of the vitiated co-flow, and this spurred further experimental investigations [103]. Fig. 6 compares the measured lift-off height [103] with that calculated by the same PDF method [94] as used for the Barlow and Frank flames (as described above). In this case a 10-species detailed mechanism is used for the hydrogen combustion. As may be seen from Fig. 6, the PDF calculations are in excellent agreement with the experimental data, with any discrepancies being well within experimental uncertainties.

This and subsequent studies [95–97,102] reveal that the fundamental stabilization mechanism in this flame is the (essentially inert) mixing between the cold fuel and the hot oxidant, followed by auto-ignition. In contrast to lifted flames in cold

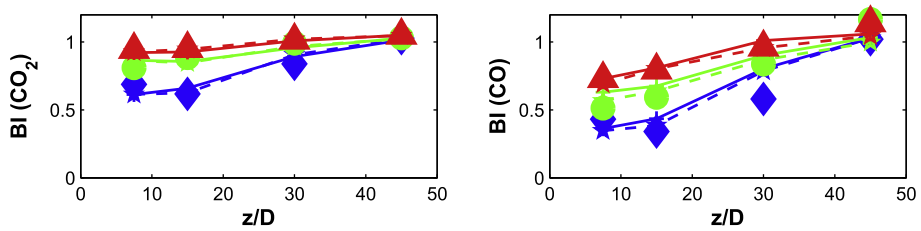

Fig. 5. Burning indices of CO_2 (left) and CO (right) versus axial distance for flames D, E and F (from top to bottom). Symbols, experimental data [34]. Lines, from PDF calculations [76] using the GRI3.0 mechanism (solid lines) and the GRI2.11 mechanism (dashed lines).

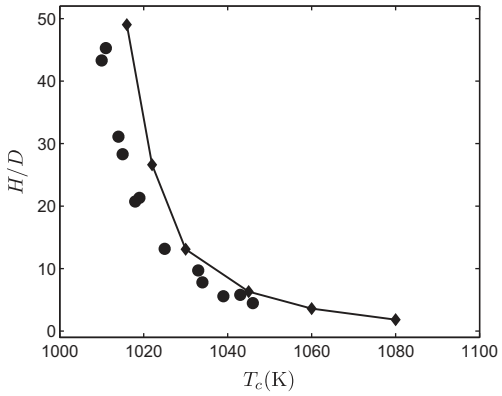

Fig. 6. Lift-off height H normalized by the jet diameter D against co-flow temperature T_c for a hydrogen/nitrogen jet flame in a vitiated co-flow: symbols, experimental data [103]; line with symbols, PDF calculations [94]. Reprinted with permission from [27]. Copyright 2011, American Institute of Physics.

co-flows, the stabilization of the flame does not depend upon flame propagation against the flow.

It is interesting to observe that in the PDF method described here and applied to the Barlow and Frank and Cabra flames, the molecular diffusivity D is not specified: that is, D is not an input parameter that needs to be specified, or indeed that can be specified. Instead, consistent with the high-Reynolds-number, cascade paradigm, the rate of molecular mixing is modeled as being determined by the large-scale turbulent motions. It is perhaps surprising that this high-Reynolds-number assumption is successful in these relatively low-Reynolds-number flames, in which visualizations and DNS reveal diffusive structures whose size is a significant fraction of the flow width.

5.4. Modeling of molecular mixing

In the composition PDF equation, molecular diffusion appears as the *conditional diffusion*

$$G_i(\widehat{\mathbf{Y}},\mathbf{x},t) \equiv \left\langle \frac{1}{\rho}\nabla\cdot(\rho D\nabla Y_i) \mid \mathbf{Y}(\mathbf{x},t)=\widehat{\mathbf{Y}}\right\rangle. \tag{17}$$

Models for this quantity are called *mixing models*, the simplest of which is the *interaction by exchange with the mean* (IEM) model [104], or, equivalently, the *linear mean square estimation* (LMSE) model [105], which is:

$$G_i(\widehat{\mathbf{Y}},\mathbf{x},t) = -\frac{1}{2}C_\phi\frac{\varepsilon}{k}(\widehat{Y}_i-\widetilde{Y}_i), \tag{18}$$

where k is the turbulent kinetic energy, ε is the mean dissipation rate, $\widetilde{\mathbf{Y}}$ is the Favre mean of the species mass fractions (all evaluated at $(\mathbf{x},t)$), and C_ϕ is a constant, generally taken to be $C_\phi = 2$. Consistent with the picture of the energy cascade at high Reynolds number, the rate of mixing is proportional to the inverse of the time scale (k/ε) of the energy-containing turbulent motions, and is independent of the molecular diffusivity, D. Another simple and popular model with similar performance is the *modified Curl* (MC) model [106–108].

PDF methods have long been criticized for not accounting for the effects of chemical reactions on molecular mixing. If simple models such as IEM and MC are used, then this criticism is fully justified. However, as now explained, more sophisticated models do account for these effects, and current research is leading to further improvements.

The first observation to make is that, if there is a very strong coupling between reaction and diffusion so that turbulent combustion occurs in a flamelet regime, then the flamelet assumption leads to a closure for the conditional diffusion. Using this observation, over 25 years ago, PDF methods were successfully applied to premixed combustion in the flamelet regime [109,110].

Similarly, for non-premixed combustion, the simplest flamelet model assumption

$$\mathbf{Y}(\mathbf{x},t) = \mathbf{Y}^{\mathrm{sfm}}(Z(\mathbf{x},t),\chi_{st}), \tag{19}$$

for a fixed, specified value of scalar dissipation, χ_{st}, leads to a closure for the conditional diffusion. The resulting modeled equation for the PDF of $\mathbf{Y}$ is equivalent to solving for the PDF of mixture fraction and then obtaining the PDF of the species from Eq. (19).

The deficiencies of the simple mixing models for reacting flows have been recognized for several decades [111], and this has led to improved models, most notably the *Euclidean minimum spanning tree* (EMST) model [90] and *multiple mapping conditioning* (MMC) [54,55].

The EMST model has an unconventional form and is difficult to analyze. However, an analysis is performed in Appendix A of the EMST model (with some simplifying assumptions) applied to non-premixed turbulent combustion. This analysis shows that, according to the model, the species evolve by an equation (Eq. (A.12)) which is very similar to the unsteady flamelet equation. This clearly demonstrates that, in the EMST model, molecular mixing is affected by reaction in a realistic way.

The IEM model yields the same mixing rate for all species, whereas DNS of both non-premixed [112] and premixed combustion [113,114] clearly shows significantly different mixing rates for different reactive species. In recent work, Richardson and Chen [114] show that the EMST model also yields different mixing rates for different species. For the low-Reynolds-number case considered, they extend the model to include differential diffu-

sion, and this model shows reasonable quantitative agreement for the mixing rates of the different species, which vary by an order of magnitude.

Even though the EMST model has proven more successful than other mixing models, it has some fundamental shortcomings, which have been recognized since its introduction [90]. These include the violation of linearity and independence principles, and its uncertain convergence as the number of particles used to represent the PDF tends to infinity.

The closure provided by MMC is also difficult to analyze, but it can be expected to make reaction affect mixing at least as realistically as EMST. Also relevant here is the model of Lindstedt and Váos [115], in which the mixing rate depends on reaction.

5.5. Large-eddy simulations using PDF methods

The idea of using PDF methods as the turbulent combustion model used in conjunction with LES goes back over 20 year [8,116,117]. Lagrangian particle/mesh methods to implement LES/PDF were pioneered by Givi and co-workers [81,118–124], with several subsequent implementations by other groups [82,125–127]. There have also been implementations [128] based on the stochastic fields approach [80,129]. Here we just make a few observations about LES/PDF as it pertains to the themes of this paper. For reviews of recent work, the reader is referred to [36,37].

The first observation is to stress the fact that in LES, as in RANS, there are large-amplitude fluctuations on the small scales, which are not resolved. Consequently, the statistical modeling of reaction and molecular diffusion on the unresolved small scales is essential and crucial. To illustrate this point, Fig. 7 shows a scatter plot of temperature versus radial position color-coded by Y_{OH} obtained from an LES/PDF calculation of the Barlow and Frank [34] flame E. The points shown are from a single row of cells in the radial direction at a single time. As may be seen, at a given location (e.g., $r/D = 1$), the temperature may vary by over 1000 K, and Y_{OH} varies over its full range.

In Lagrangian particle implementations, the particle position $\mathbf{X}^*(t)$ and mass fractions $\mathbf{Y}^*(t)$ evolve by three processes—advection, reaction, and molecular diffusion. In LES/PDF, as in RANS/PDF, reaction is implemented exactly through the ODE $d\mathbf{Y}^*/dt = \widehat{\mathbf{S}}(\mathbf{Y}^*)$. In LES/PDF, advection of particles is by the resolved velocity and a model for the residual turbulent velocity; whereas in RANS/PDF advection is by the mean velocity and a model for the fluctuating velocity. Perhaps the largest differences are in the treatment of molecular diffusion, and these are now outlined.

First, while the fluctuations in LES/PDF are large (as illustrated in Fig. 7), they are not as large as in RANS/PDF. In LES/PDF, localness in physical space is accompanied by some degree of localness in species space. Consequently, the modeling of molecular mixing may in this sense be less difficult than in RANS/PDF. For example, in recent LES/PDF calculations [130] using the simple IEM mixing model, it is found that the modeled conditional diffusion exhibits complex, nonlinear behavior, similar to that observed in DNS of the same flame (whereas the IEM model in RANS/PDF yields linear behavior).

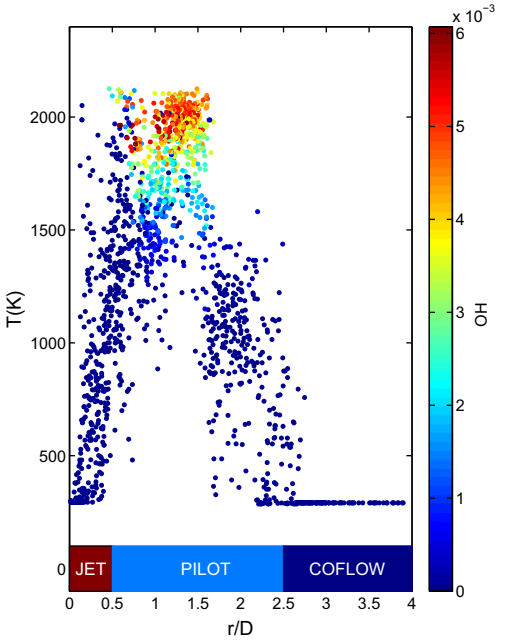

Fig. 7. Scatter plot of temperature versus radius r (normalized by the jet diameter D), color-coded by the mass fraction of OH, from an LES/PDF calculation of the Barlow and Frank flame E at the axial location $x/D = 15$. The points are from the computational particles in a single row of cells in the radial direction, at one time. There are 80 cells over the radial range shown, which is a fraction of the radial extent of the solution domain (from H. Wang, private communication).

Second, in RANS/PDF, the direct effects of molecular diffusion on the mean mass fractions are negligible, and molecular mixing is modeled as occurring at a rate determined by the turbulence, independent of the molecular diffusivity, D. In a typical LES of a laboratory flame (or of a DNS), the direct effects of molecular diffusion on the resolved mass fractions are very significant, and dominant at high temperatures [38]. It is nontrivial to incorporate the direct effects of molecular diffusion in Lagrangian particle methods, but such implementations have been developed, including the capability to treat differential diffusion [131,132].

Third, it appears that it is more challenging in LES than in RANS to model accurately the

mixing rate [133]. This may be because the range of scales—resolved-to-dissipative—is smaller; and (relatedly) it may also be because of the stronger, direct effects of the molecular diffusivity.

In industrial applications, typically the Reynolds numbers are significantly larger than in laboratory flames (e.g., by an order of magnitude), and consequently there is a larger range of scales, and the direct effects of molecular diffusivity at the resolved scales are smaller. Consequently, there is a serious concern that LES models developed and tested against laboratory and DNS data may not be reliable when applied to industrial problems. With the LES resolution typically used, for laboratory flames and DNS, a good fraction of the molecular mixing is resolved, and the unresolved processes to be modeled are dominantly at the dissipative scales; whereas in LES applied to industrial problems, typically only a small fraction of the molecular mixing is resolved, and the unresolved processes are dominantly in the inertial range of scales.

An issue with LES/PDF is its computational cost. This has been quantified in a series of simulations [134,135] of the Barlow and Frank piloted jet flame D. Taking LES using a simple flamelet model as one unit of cost, the cost of LES/PDF using a simple flamelet model (based solely on mixture faction) is 3.2 units. This increase in cost is due to the work required to perform advection and mixing on the 40 computational particles per cell. For LES/PDF with the methane chemistry represented by a 16-species mechanism, the cost is 8.6 units; and when a 38-species mechanism is used the cost is 17.3 units. In the latter case, 65% of the total time is taken in the reaction fractional step. In comparison, the cost of a RANS/PDF calculation of this flame using a 16-species mechanism is one fifth of the cost of LES using a simple flamelet model, and a factor of 45 less than an LES/PDF calculations using the same 16-species mechanism. Further quantification of the computational costs and issues, including parallelization, are provided in [134,135].

Based on these relative costs, we make the following observations.

1. In simple combustion regimes, where flamelet-like models provide an adequate description of the turbulence-chemistry interactions, there is a clear cost penalty in using LES/PDF. The benefit of LES/PDF is therefore in the more challenging regimes, where flamelet-like models are inaccurate.
2. For the case of LES/PDF with 38 species, the thermochemical information content is a factor of 760 greater than in the LES/flamelet simulation (i.e., 38 species mass fractions for 40 particles per cell, compared to the mean and variance of mixture fraction for each cell). The fact that the computational cost is greater by only a factor of 17.3 demonstrates the progress that has been made in the development of efficient algorithms.
3. The relative cost of LES/PDF is likely to decrease as further algorithmic advances are made, including the use of adaptation. For flame D, it is obviously wasteful to describe the uniform, inert, co-flowing air stream by a PDF method using 38-species chemistry!
4. The cost increase in advancing from flamelet-like models to PDF methods is small compared to the cost of advancing from RANS to LES.

5.6. Other PDF-like models

Since its original development 10 years ago [54], multiple mapping conditioning (MMC) has evolved, with different variants, implementations and viewpoints [55]. One viewpoint is that the stochastic variant of MMC amounts to a PDF method, with a Lagrangian particle implementation, involving additional "reference variables", which are used in the modeling of mixing. Whereas EMST makes the mixing local in the species space, MMC makes mixing local in the space of the reference variables. Such implementations of MMC have all the characteristics of PDF-like models. Recent work on stochastic MMC includes [136–141] and is reviewed in [55].

In the linear-eddy model (LEM) [56,57] and in the one-dimensional turbulence (ODT) model [58,59], fluid properties are represented (with full resolution) along some lines within the flow, and hence there is some representation of the small-scale processes. LEM and ODT have several similarities to PDF methods (implemented as a Lagrangian particle method, and using the EMST mixing model). Specifically:

- Both are Monte Carlo methods in which the composition of the fluid is represented at discrete points—fixed mesh points in LEM and ODT, Lagrangian particles in PDF.
- Reaction is treated directly according to $d\mathbf{Y}/dt = \widehat{\mathbf{S}}(\mathbf{Y})$.
- Molecular mixing occurs by an exchange of species between neighboring points—adjacent mesh points in LEM and ODT, nearest neighbors in species-space in the EMST model.
- Both are applicable in both the RANS and LES contexts.

The principal differences are that in PDF methods convection is treated directly and naturally by the motion of the particles; and in LEM and ODT molecular diffusion is treated directly and naturally via the unsteady diffusion equation (with the effects of turbulence on mixing being repre-

sented by triplet maps). Because of these similarities, many of the considerations pertaining to PDF methods apply equally to LEM and ODT.

Recent work on LEM and ODT includes [142–147], and reviews are provided by [57,59].

6. Manifolds in species space

As illustrated above, several different low-dimensional manifolds arise in models of turbulent combustion. In this section we address fundamental questions about modeling turbulent combustion from the perspective of these manifolds. Before these questions are posed and discussed, we start by introducing some terminology and a classification of the manifolds used.

6.1. Representation of manifolds

In general, an m-dimensional manifold in the n_s-dimensional species space (with $n_s > m \geqslant 1$) can be described by a function $\mathbf{Y}^M(\boldsymbol{\theta})$, which is a mapping from the m parameters $\boldsymbol{\theta} = \{\theta_1, \theta_2, \ldots, \theta_m\}$ to the species space. To simplify the discussion, and to give physical meaning to the parameters, we take the parameters to be a selected set of m species. Thus, we partition the species into a set of $n_r = m$ *represented species* and the remaining $n_u = n_s - n_r$ *unrepresented species*. With the species being ordered so that the represented species are before the unrepresented species, the mass fractions can be written

$$\mathbf{Y} = \begin{bmatrix} \mathbf{Y}^r \\ \mathbf{Y}^u \end{bmatrix}, \tag{20}$$

where $\mathbf{Y}^r$ and $\mathbf{Y}^u$ are n_r and n_u vectors in the represented and unrepresented subspaces, respectively. Now, with $\mathbf{Y}^r$ being used as the parameters, the manifold can be expressed as the compositions $\mathbf{Y}$ satisfying

$$\mathbf{Y} = \mathbf{Y}^M(\mathbf{Y}^r) = \begin{bmatrix} \mathbf{Y}^r \\ \mathbf{Y}^m(\mathbf{Y}^r) \end{bmatrix}, \tag{21}$$

where the function $\mathbf{Y}^m(\mathbf{Y}^r)$ is a mapping from the represented subspace to the unrepresented subspace. A manifold represented by the last part of Eq. (21) is said to be a graph of a function. (Note the distinction between $\mathbf{Y}^M$ and $\mathbf{Y}^m$, which are n_s and n_u vectors, respectively.)

Given a manifold defined by $\mathbf{Y}^m(\mathbf{Y}^r)$ and a composition $\mathbf{Y}$ (not necessarily on the manifold), as illustrated in Fig. 8, we can decompose $\mathbf{Y}$ as

$$\mathbf{Y} = \begin{bmatrix} \mathbf{Y}^r \\ \mathbf{Y}^u \end{bmatrix} = \begin{bmatrix} \mathbf{Y}^r \\ \mathbf{Y}^m(\mathbf{Y}^r) + \mathbf{y} \end{bmatrix}, \tag{22}$$

where

$$\mathbf{y} \equiv \mathbf{Y}^u - \mathbf{Y}^m(\mathbf{Y}^r) \tag{23}$$

is the departure from the manifold (in the unrepresented subspace). The conservation equations for $\mathbf{Y}^r$ and $\mathbf{y}$ are derived and discussed in Section 6.3 and in Appendix B.

We introduce the following notation: upper-case Roman letters are used to denote components of represented quantities (e.g., Y^r_I for $1 \leqslant I \leqslant n_r$), and lower-case Greek letters denote components of unrepresented quantities (e.g., Y^u_α for $1 \leqslant \alpha \leqslant n_u$). When needed for clarity, we use $\hat{\mathbf{Y}}^r$, $\hat{\mathbf{Y}}^u$ and $\hat{\mathbf{y}}$ as sample-space variables corresponding to $\mathbf{Y}^r$, $\mathbf{Y}^u$ and $\mathbf{y}$.

Fig. 8 illustrates a simple 1D manifold. In general there are n_r tangent vectors $\mathbf{T}_I \equiv \partial \mathbf{Y}^M / \partial Y^r_I$ which together span the local n_r-dimensional tangent subspace $\mathcal{T}$. The orthogonal complement of $\mathcal{T}$ is the n_u-dimensional normal subspace $\mathcal{N}$.

The chemical source term $\mathbf{S}$ can be decomposed as

$$\mathbf{S} = \begin{bmatrix} \mathbf{S}^r \\ \mathbf{S}^u \end{bmatrix} = \mathbf{S}^{\parallel} + \begin{bmatrix} 0 \\ \mathbf{S}^{\angle} \end{bmatrix}, \tag{24}$$

where $\mathbf{S}^r$ and $\mathbf{S}^u$ are in the represented and unrepresented subspaces, respectively; $\mathbf{S}^{\parallel}$ is in the tangent space and $\mathbf{S}^{\angle}$ is in the unrepresented subspace (see Fig. 8).

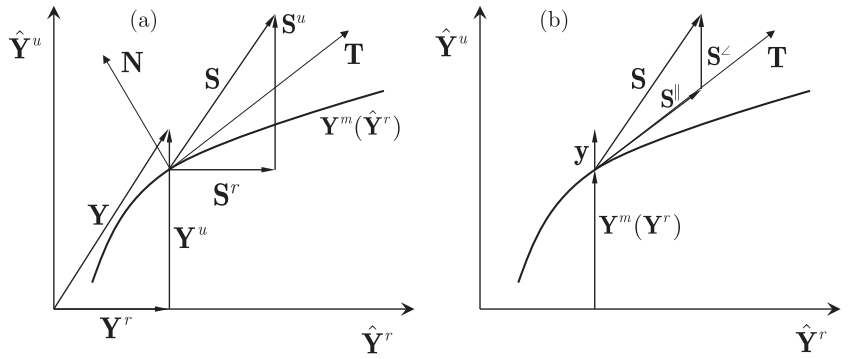

Fig. 8. Sketch showing a 1D manifold defined by $\mathbf{Y}^u = \mathbf{Y}^m(\mathbf{Y}^r)$ and (a) the tangent and normal vectors; the decomposition of $\mathbf{Y}$ and $\mathbf{S}$ into components in the represented and unrepresented subspaces (b) the decomposition $\mathbf{Y}^u = \mathbf{Y}^m(\mathbf{Y}^r) + \mathbf{y}$; and the decomposition of $\mathbf{S}$ in terms of $\mathbf{S}^{\parallel}$ and $\mathbf{S}^{\angle}$.

We define

$$K_{\alpha,IJ} \equiv \frac{\partial^2 Y^m_\alpha}{\partial Y^r_I \partial Y^r_J}, \tag{25}$$

and loosely refer to it as the "curvature". There is a very important distinction between a *plane* and a *curved* manifold. For a plane manifold we can write

$$\mathbf{Y}^m = \mathbf{Y}^{m0} + \mathbf{A}\mathbf{Y}^r, \tag{26}$$

where $\mathbf{Y}^{m0}$ is a constant vector, and $\mathbf{A}$ is a constant $n_u \times n_r$ matrix. For such a plane manifold, the tangent and normal subspaces are the same everywhere (and known in terms of $\mathbf{A}$), and the curvature is zero everywhere. In contrast, for a curved manifold, in general the tangent and normal subspaces vary on the manifold, and the curvature $\mathbf{K}$ is non-zero.

For the simplest possible case of a 1D manifold in 2-space, Fig. 9 illustrates some properties of "good" and "bad" manifolds. For all realizable values of $\mathbf{Y}^r$, a good manifold exists, is single-valued, and is realizable. These are the minimum requirements of a manifold in order for it to be used in a turbulent combustion computation without arbitrariness or *ad hoc* corrections. The level of continuity required depends on the particular implementation, but obviously smoothness is desirable.

6.2. Classification of manifolds

We now classify the different types of manifolds used in turbulent combustion. Table 1 provides a summary of this classification, with explanations and details provided in the following subsections.

6.2.1. Skeletal manifolds

Given a detailed mechanism containing hundreds or thousands of species, the usual first step towards a more tractable description is to construct a skeletal mechanism by simply omitting some species and reactions, those which are deemed to have a negligible effect on the combustion problem being studied. Viewed in the current framework, the retained and omitted species are identified as the represented and unrepresented species, respectively, and the complete neglect of the unrepresented species defines the skeletal manifold by

$$\mathbf{Y}^M = \begin{bmatrix} \mathbf{Y}^r \\ 0 \end{bmatrix}, \tag{27}$$

or, equivalently,

$$\mathbf{Y}^m(\mathbf{Y}^r) = 0. \tag{28}$$

The skeletal manifold thus defined is a good, plane manifold.

Methods to rank species for retention include, for example, the *directed relation graph* (DRG) method [148], the DRG method with error propagation (DRG-EP) [149,150], and earlier proposals [151–155].

Table 1
Classification of the various low-dimensional manifolds used in turbulent combustion models and their associated methods. Definitions and references are provided in the text.

Type of manifold	Examples and associated methods
Skeletal	DRG, DRG-EP
Thermodynamic	Equilibrium, CEM, RCCE, GALI
Reaction	QSSA, ILDM, TGLDM, ICE-PIC, CSP, LoI
Diffusion	Inert mixing
Reaction-diffusion	SFM, FPV, FGM, FPI, REDIM
Conditional	CMC, MMC
Empirical	PCA, MARS, Isomap

6.2.2. Thermodynamic manifolds

We define a thermodynamic manifold to be a manifold that is determined by the thermodynamic properties of the system, which are known functions of $\mathbf{Y}$. As a simple example, the equilibrium manifold shown in Fig. 2 is a 1D thermody-

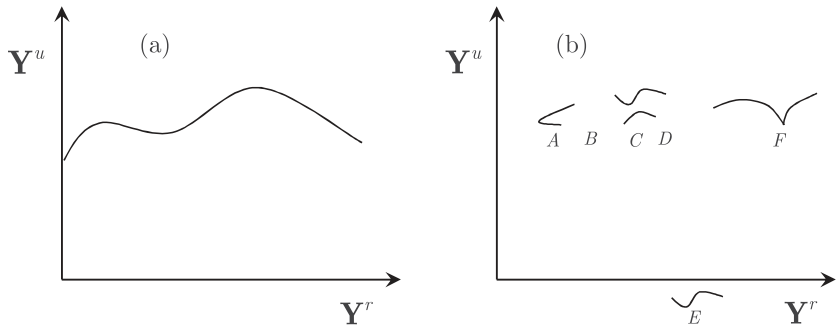

Fig. 9. Sketch of (a) a "good" manifold and (b) a "bad" manifold. At the indicated locations, the bad manifold: (A) is folded; (B) does not exist; (C) is multi-valued; (D) is discontinuous; (E) is not realizable; (F) is not smooth.

namic manifold, and we can take N_2 to be the single represented species. In this example, by definition, for each value of Y_{N_2}, the corresponding point on the equilibrium manifold is the composition of maximum entropy consistent with the constraints imposed by the elements mass fractions and enthalpy, which are known functions of Y_{N_2}.

More generally, we consider the *constrained equilibrium manifold* (CEM) in which additional constraints are imposed corresponding to represented species, or linear combinations of species. This is the manifold used in the rate-controlled constrained equilibrium method (RCCE) [156,157], which is seeing renewed use in turbulent combustion calculations [135,158–161]. The CEM is a good curved manifold.

A *greedy algorithm with local improvement* (GALI) [159,162] has been developed to select appropriate represented species for RCCE. The study of [159] confirms the hope and expectation that as the dimension of the manifold increases so also does the accuracy with which it can represent turbulent combustion. For the particular case of methane combustion studied, the error decreases from over 100% for $n_r = 2$ and 3, to less than 1% for $n_r = 11$.

6.2.3. Reaction manifolds

For a homogeneous system, the species conservation equation (Eq. (1)) reduces to the autonomous set of ordinary differential equations

$$\frac{d\mathbf{Y}(t)}{dt} = \widehat{\mathbf{S}}(\mathbf{Y}(t)), \tag{29}$$

describing the change of composition due to reaction in isobaric, adiabatic autoignition. By definition, *reaction manifolds* are based on this equation, or on the properties of the chemical source term $\widehat{\mathbf{S}}(\mathbf{Y})$. As now described, examples include: trajectory-generated low-dimensional manifolds (TGLDM) [163]; quasi-steady-state (QSS) manifolds [164]; intrinsic low-dimensional manifolds (ILDM) [165]; and those implied by computational singular perturbation (CSP) [166].

From an initial condition $\mathbf{Y}^0$, the solution to Eq. (29) is a trajectory in the species space from $\mathbf{Y}^0$ to the equilibrium composition. This trajectory is a one-dimensional manifold, which can be parameterized by time, entropy, or the mass fraction of a major species (provided that it varies monotonically along the trajectory). Instead of a single initial condition, $\mathbf{Y}^0$, we can consider as initial conditions all points on an $(m-1)$-dimensional manifold. The trajectories emanating from these initial conditions form an m-dimensional trajectory-generated low-dimensional manifold (TGLDM) [163]. The ICE-PIC method ([167,168]) employs an m-dimensional TGLDM generated by an $(m-1)$-dimensional CEM on the boundary of the realizable region of the represented species.

TGLDMs are good, curved manifolds, which inherit the smoothness properties of the manifolds from which they are generated. They are said to be *invariant* (with respect to Eq. (29)), meaning that solutions to Eq. (29) from initial conditions on the manifold remain on the manifold. Equivalently, the chemical source term is a vector in the tangent space of the manifold, so that $\mathbf{S}^{\angle}$ is zero.

The quasi-steady-state approximation (QSSA), frequently used in reduced mechanisms (e.g., [169–171]), also implies a reaction manifold. The represented and unrepresented species are identified with the non-QSS species and the QSS species, respectively. Then, the QSS approximation is that the components of the chemical source term corresponding to the unrepresented species are zero. This can be written

$$\mathbf{F}^T\widehat{\mathbf{S}}(\mathbf{Y}) = 0, \tag{30}$$

where the $n_s \times n_u$ matrix is

$$\mathbf{F} = \begin{bmatrix} 0 \\ \mathbf{I} \end{bmatrix}, \tag{31}$$

where $\mathbf{I}$ is the $n_u \times n_u$ identity. Or, with i corresponding to a QSS species, the QSSA and Eq. (5) yield

$$0 = \widehat{S}_i = S_i^+ - Y_i/\tau_{(i)}, \tag{32}$$

leading to

$$Y_i = S_i^+\tau_{(i)}. \tag{33}$$

If the production rate S_i^+ and the consumption time scale τ_i are determined by the represented species, then Eq. (33) explicitly determines a unique, realizable value for the mass fraction Y_i of the unrepresented species. More generally, both S_i^+ and τ_i may also depend on the unrepresented species, so that Eq. (33) becomes a coupled set of n_u non-linear algebraic equations for the mass fractions of the unrepresented species in terms of the mass fractions of the represented species. Solutions to such equations may not exist, may not be unique, or may not be realizable, and these difficulties do sometimes arise in practice. Consequently a QSS manifold may not be "good". A linearized version of QSSA has been developed [172] which ensures good manifolds.

Methods to identify appropriate QSS species include CSP [166,173,174] and *level of importance* (LoI) [24,175].

The n_r-dimensional intrinsic low-dimensional manifolds (ILDM) is also defined by Eq. (31), but with a different definition of the matrix $\mathbf{F}$. Specifically, the columns of $\mathbf{F}$ span the invariant subspace corresponding to the n_u eigenvalues of the Jacobian $\mathbf{J}$ (Eq. (8)) with smallest real parts. In this way, instead of the n_u QSS species being specified, the n_u "fastest" linear combination of reactions is determined locally (without the need for

any specification). Because the invariant subspace can change discontinuously (where eigenvalues cross), an ILDM may not be "good", and indeed examples of bad behavior have been encountered [167].

6.2.4. Diffusion manifolds

We consider the inert mixing (according to Eq. (1)) of S homogeneous streams with linearly independent compositions $\mathbf{Y}^{(s)}$, for $1 \leqslant s \leqslant S \geqslant 2$. As is well known [176], the compositions that occur in inert mixing (with equal diffusivities) are confined to the convex hull of the S points $\mathbf{Y}^{(s)}$ in the species space. This is a plane n_r-dimensional manifold, for $n_r = S - 1$, which can be parameterized by n_r mixture fractions or linearly independent species.

6.2.5. Reaction-diffusion manifolds

Here we define a reaction-diffusion manifold to be a manifold obtained as the solution of ordinary or partial differential equations which contain a diffusion term in addition to the chemical source term. The most familiar example of a reaction-diffusion manifold is the steady flamelet manifold obtained as the solution to Eq. (9), an example of which is shown in Fig. 3. Similarly, the approaches of *flamelet-generated manifolds* (FGM) [48] and *flame prolongation of ILDM* (FPI) [49] obtain manifolds as solutions of the conservation equations for particular laminar flames.

The differential equations governing laminar flames can be considered in physical space (e.g., Eq. (1)) or in a space of parameters such as mixture fraction and reaction progress variable (e.g., Eq. (9)). In their REDIM method, Bykov and Maas [50,51] generalize the latter approach and consider a reaction-diffusion equation analogous to Eq. (9) but in terms of m general parameters, leading to an m-dimensional manifold. In place of the scalar dissipation, in REDIM an m-vector coefficient is specified, which determines the magnitude of the diffusion term in the parameter space. (While REDIM stands for "reaction-diffusion manifold", here we use the latter term more generally.) The earlier "phase space ILDM" method (PS-ILDM) [177] is based on similar ideas.

In general, reaction-diffusion manifolds are "good", because the diffusion terms and the associated boundary conditions guarantee the existence of smooth manifolds. Compared to reaction manifolds, reaction-diffusion manifolds may be considered to provide a better approximation for the compositions that occur in turbulent flames because the effects of both reaction and molecular diffusion are accounted for. However, it should be appreciated that a particular coupling between reaction and diffusion is assumed, and this is parameterized by a small number of parameters; zero for an unstrained premixed laminar flame, one in the steady flamelet model, and a constant m-vector in REDIM. As discussed further below, it is questionable whether such simple couplings adequately describe the complexities of turbulent combustion.

6.2.6. Conditional manifolds

The manifolds described above are applicable to both laminar and turbulent flows, and they are *global*, in the sense that the same manifold is used everywhere (i.e., for all $\mathbf{x}$ and t). In contrast, the *conditional manifolds* considered here apply only to turbulent flows, and they are *local* in the sense that, in general, they depend on $\mathbf{x}$ and t. These conditional manifolds arise in conditional moments closures (CMC) [60,61] and in multiple mapping conditioning (MMC) [54,55].

The conditional manifold $\mathbf{Y}^u = \mathbf{Y}^{\mathrm{cm}}$ is defined simply as the expectation of $\mathbf{Y}^u$ conditional on $\mathbf{Y}^r$. To make this definition precise, we introduce sample-space variables $\widehat{\mathbf{Y}}^r$ corresponding to the represented composition $\mathbf{Y}^r(\mathbf{x},t)$. Then, the conditional manifold is defined as the conditional expectation

$$\mathbf{Y}^{\mathrm{cm}}(\widehat{\mathbf{Y}}^r, \mathbf{x}, t) \equiv \langle \mathbf{Y}^u(\mathbf{x},t) \mid \mathbf{Y}^r(\mathbf{x},t) = \widehat{\mathbf{Y}}^r \rangle. \tag{34}$$

In CMC it is observed that $\mathbf{Y}^{\mathrm{cm}}$ typically depends primarily on $\widehat{\mathbf{Y}}^r$, with a much weaker dependence on position, $\mathbf{x}$. This dependence on $\mathbf{x}$ is likely to become yet weaker as the number of represented variables increases.

Also in contrast to the previous manifolds discussed, rather than being determined separately in a pre-processing stage, in CMC and MMC the conditional manifold is determined as part of the turbulent combustion model calculation. For the simplest, idealized case of statistically homogeneous and stationary turbulent combustion, the most basic CMC equation determining the conditional manifold is [54,61]

$$0 = \langle \chi_{IJ} | \widehat{\mathbf{Y}}^r \rangle \frac{\partial^2 \mathbf{Y}^{\mathrm{cm}}}{\partial \widehat{Y}^r_I \partial \widehat{Y}^r_J} + \mathbf{S}^{\angle}(\widehat{\mathbf{Y}}^r), \tag{35}$$

where $\langle \chi_{IJ} | \widehat{\mathbf{Y}}^r \rangle$ is the conditional scalar dissipation of the represented species, and $\mathbf{S}^{\angle}$ is the component of $\mathbf{S}$ in the unrepresented subspace and not in the tangent space (see Eq. (24) and Fig. 8). See Appendix B for a fuller explanation. Interestingly, Eq. (35) is precisely the form of reaction-diffusion equation solved in REDIM, and the CMC analysis identifies the conditional scalar dissipation as the appropriate diffusivity matrix.

6.2.7. Empirical manifolds

The manifolds described above are all theoretical constructs, based on the governing conservation equations and thermochemistry. Their application to turbulent combustion involves

sweeping assumptions. In contrast, *empirical manifolds* are constructed based on samples of the compositions observed in turbulent combustion, either in experiments or in DNS.

We focus here on empirical manifolds based on DNS data, which, compared to experimental data, has several advantages: the mass fractions $\mathbf{Y}$ of all species are known; the numerical errors in good-quality DNS are much smaller than the measurement errors in experiments; and the chemical source term $\mathbf{S}$ is available, in addition to the mass fractions $\mathbf{Y}$. On the other hand, DNS is limited to relatively low Reynolds numbers and simple chemical mechanisms.

The realistic hope and expectation is not that compositions occurring in turbulent combustion lie exactly on a low-dimensional manifold, but rather that they lie close to one. Given an empirical manifold (expressed as $\mathbf{Y}^M(\mathbf{Y}^r)$ or as $\mathbf{Y}^m(\mathbf{Y}^r)$, Eq. (21)), an observed composition $\mathbf{Y}$ can be decomposed as

$$\mathbf{Y} = \begin{bmatrix} \mathbf{Y}^r \\ \mathbf{Y}^u \end{bmatrix} = \mathbf{Y}^M(\mathbf{Y}^r) + \begin{bmatrix} 0 \\ \mathbf{y} \end{bmatrix} = \begin{bmatrix} \mathbf{Y}^r \\ \mathbf{Y}^m(\mathbf{Y}^r) + \mathbf{y} \end{bmatrix}, \tag{36}$$

where

$$\mathbf{y} \equiv \mathbf{Y}^u - \mathbf{Y}^m(\mathbf{Y}^r), \tag{37}$$

is the departure of $\mathbf{Y}$ from the manifold. Thus, an empirical manifold can be constructed from an ensemble of N observations of $\mathbf{Y}$ by minimizing some measure of the departures $\mathbf{y}$ of the observations from the manifold.

By far the simplest empirical manifold is the plane manifold obtained from the principal component analysis (PCA) of the data [178]. Simply by performing the singular value decomposition of the $N \times n_s$ matrix of observed mass fractions, one can determine both the "best-fit" n_r-dimensional plane manifold, and a suitable set of n_r represented species for its parameterization. The result can be compactly expressed by Eq. (26).

Sutherland and co-workers [178–181] have examined PCA manifolds based on data from experiments, DNS and from ODT simulations. Yang and Pope [182] performed similar examinations based on the DNS data from CO/H_2 and ethylene non-premixed jet flames [112,183]. The main question to address is: for a given data set of N samples of $\mathbf{Y}$, how closely does the PCA manifold of dimension n_r approximate the data? This question can be addressed by examining the r.m.s. distance of the data from the manifold. Specifically, for species i we define ϵ_i to be the r.m.s. of the departure $Y_i - Y_i^M$ normalized by the standard deviation of Y_i. Fig. 10 shows this normalized measure of the departure for two representative species, CO_2 and H, obtained from the DNS of Hawkes et al. [112]. The data are taken from several times in the highest-Reynolds-number simulation, in which there is substantial local extinction and reignition. As may be seen from Fig. 10, eight dimensions are needed (i.e., $n_r \geqslant 8$) in order to reduce these departures from the manifold to below 5%.

It is possible that the DNS data lie closer to a manifold parameterized by variables other than mass fractions. In particular, a prediction of the steady flamelet model is that, for the subset of samples close to stoichiometric, the species mass fractions are given by $\mathbf{Y} = \mathbf{Y}^{\mathrm{sfm}}(Z_{st},\chi)$, i.e., $\mathbf{Y}$ depends solely on χ. For the same data considered above, but conditioned on Z being close to stoichiometric, Fig. 11 shows scatter plots of the mass fraction of CO_2 versus χ (left plot) and versus the first principal component, η_1 (right plot). (The first principal component is the distance from the mean in species space in the direction of the first singular vector in the PCA analysis, i.e., in the direction of greatest variation.) Evidently, as should be expected, and as previously observed [178,181], the steady flamelet model is not applicable to this case, and there is essentially no correlation between Y_{CO_2} and χ. The one-dimensional PCA provides a much better representation of the data, with the normalized r.m.s. departure ϵ_{CO_2} being 33%.

Representing and determining "best-fit" curved manifolds is much more challenging than PCA. The most promising approach is *multivariate adaptive spline regression* (MARS) [181,184]. In fact, in the present context, MARS can be used for two different purposes. First, MARS can be used to approximate non-linear functions such as the chemical source term $\mathbf{S}$ on a plane manifold; second, it can be used to approximate a curved manifold by representing $\mathbf{Y}^m(\mathbf{Y}^r)$. In this latter case, the curved empirical manifold obtained from MARS is an estimate of the conditional manifold.

Fig. 12 compares the departures from the PCA and MARS manifolds for the DNS data of the CO/H_2 flame [112] and of the ethylene flame [183]. In this case, the normalized measure of error ϵ is the average over all species of the r.m.s. departure of the species mass fraction from the manifold, normalized by the greater of the standard deviation of that species mass fraction and 10^{-3}. (This normalization prevents small errors in trace species from making a disproportionate contribution.) As expected, for a given number of represented species n_r, the departures are smaller for MARS than for PCA. Also as may be expected, to achieve a departure less than a given level, more represented species are required for the ethylene flame (which involves 22 species) than for the CO/H_2 flame (which involves 11 species). For MARS, to achieve less than 5% departure, seven represented species are required for ethylene, and just two for CO/H_2.

Another approach that has been used to identify curved manifolds is *isomap* [185,186]. This

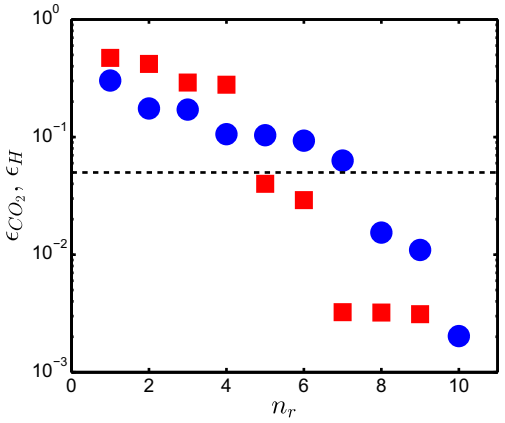

Fig. 10. Normalized r.m.s. departures of Y_{CO_2} (circles) and Y_H (squares) from the PCA manifold of dimension n_r determined from DNS data of a CO/H_2 flame [112]. The dashed line shows the 5% level (from [182]).

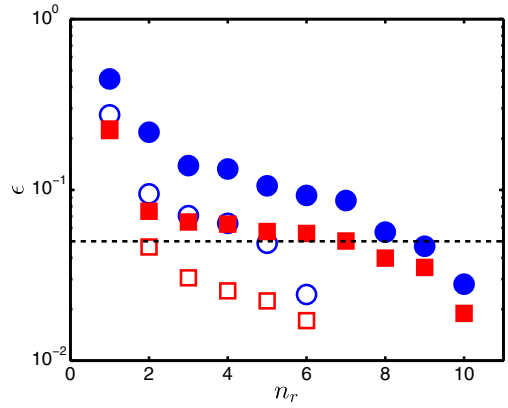

Fig. 12. Average normalized r.m.s. departures from the PCA manifold (circles) and from the MARS manifold (squares) of dimension n_r for the DNS data from the CO–H_2 flame [112] (open symbols) and from the ethylene flame [183] (solid symbols). The dashed line shows the 5% level (from [182]).

technique assumes that all data points are exactly on the manifold. In turbulent combustion, the expectation is that compositions lie close to (but not exactly on) a low-dimensional manifold. Hence, regressions techniques such as MARS appear more appropriate than interpolation techniques such as *isomap*.

The principal conclusions from studies of empirical manifolds are:

1. Plane empirical manifolds are simple to represent, exploit and determine using principal component analysis (PCA).
2. For a plane manifold to represent the species mass fractions accurately, quite high dimensions can be required. Based on the measure ϵ of the departure shown in Fig. 12, to achieve 5% accuracy, 5 and 9 dimensions are needed for the CO/H_2 and ethylene flames, respectively.
3. In several instances [178,182], it is found that a low-dimensional PCA manifold provides a better approximation than the steady flamelet manifold.
4. Curved empirical manifolds are much more difficult to represent and estimate. MARS is the most promising approach, and this yields an estimate of the conditional manifold. For the DNS data considered here, 5% accuracy is achieved with 2-and 7-dimensional curved manifolds for the CO/H_2 and ethylene flames, respectively.

It should be appreciated that the DNS data examined here are from relatively simple cases—non-premixed flames between two uniform streams, with no heat loss, and with simple 11- and 22-species chemistry for the CO/H_2 and ethyl-

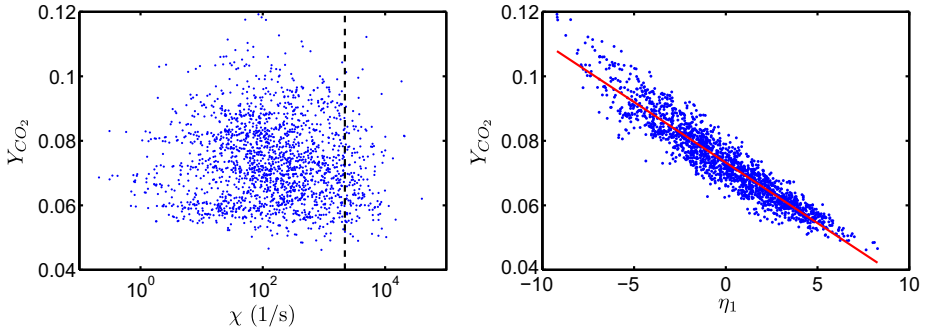

Fig. 11. For DNS data of [112], conditioned on mixture fraction Z being close to its stoichiometric value Z_{st}, scatter plots of the mass fraction of CO_2 vs. scalar dissipation (left); and vs. the first principal component, η_1 (right). The dashed line on the left plot is the extinction value of the scalar dissipation. The line on the right plot is the 1D PCA manifold (from [182]).

ene flames, respectively. The fact that the DNS data are not well approximated by very-low-dimensional empirical manifolds casts serious doubt on the applicability of flamelet-like models to these flames, and yet more so to the more complex flames encountered in applications (with more complex chemistry, more and inhomogeneous streams, heat loss, etc.).

6.3. Conservation equations on manifolds

In the previous section on empirical manifolds, we consider what might be called *a priori* testing of the low-dimensional manifold hypothesis. That is, based on DNS data obtained using chemistry with n_s species, we can examine the hypothesis that the mass fractions that occur in the flow considered lie on (or close to) an n_r-dimensional manifold $\mathbf{Y}^M(\mathbf{Y}^r)$ (for some small value of n_r). One motivation for the present section is to consider *a posteriori* testing of the hypothesis. That is, a *reduced DNS* can be performed in which conservation equations are solved for $\mathbf{Y}^r(\mathbf{x},t)$ instead of for $\mathbf{Y}(\mathbf{x},t)$. Then the accuracy of the low-dimensional manifold hypothesis can be tested by comparing statistics obtained from the reduced DNS with those from the full DNS (based on all n_s species). A turbulent combustion model using the low-dimensional manifold hypothesis cannot be expected to provide better accuracy than the reduced DNS. Computer power has now reached the point at which this *a posteriori* testing is feasible for DNS of turbulent combustion.

The conservation equation for $\mathbf{Y}^r(\mathbf{x},t)$ follows trivially from Eq. (1):

$$\frac{D\mathbf{Y}^r}{Dt} = \frac{1}{\rho}\nabla\cdot(\rho D\nabla\mathbf{Y}^r) + \mathbf{S}^r, \tag{38}$$

where the chemical source term is decomposed as

$$\mathbf{S} = \widehat{\mathbf{S}}(\mathbf{Y}) = \begin{bmatrix}\mathbf{S}^r\\ \mathbf{S}^u\end{bmatrix} = \begin{bmatrix}\widehat{\mathbf{S}}^r(\mathbf{Y})\\ \widehat{\mathbf{S}}^u(\mathbf{Y})\end{bmatrix}. \tag{39}$$

Note that Eq. (38) is not closed, in the sense that $\mathbf{S}^r$ is not known in terms of $\mathbf{Y}^r$, but instead is a function also of $\mathbf{Y}^u$. (The diffusivity also depends on $\mathbf{Y}^u$, but this is a less serious problem, which is not considered further.)

The simplest assumption that leads to a closed set of equations is that the compositions $\mathbf{Y}$ that occur lie exactly on the manifold, i.e., $\mathbf{Y} = \mathbf{Y}^M(\mathbf{Y}^r)$, or, equivalently, $\mathbf{y} = 0$. With this assumption we have

$$\mathbf{S}^r = \widehat{\mathbf{S}}^{r,m}(\mathbf{Y}^r) \equiv \widehat{\mathbf{S}}^r(\mathbf{Y}^M(\mathbf{Y}^r)). \tag{40}$$

With very few exceptions, this assumption is generally made when any type of reduced chemistry is used (e.g., with QSSA reduced mechanisms used in laminar or turbulent flame computations). However, as now explained, for turbulent combustion, the assumption that $\mathbf{Y}$ is exactly on the manifold is untenable [176]; and the complete neglect of the non-zero perturbations $\mathbf{y}$ in Eq. (40) is, in Lam's words [187] "unjustified in general".

The conservation equation for $\mathbf{y}$ is again deduced directly from Eq. (1). This is done in Appendix B, where the notation is fully explained. Briefly, the result is

$$\frac{Dy_\alpha}{Dt} - \frac{1}{\rho}\nabla\cdot(\rho D\nabla y_\alpha) \equiv \chi_{JK}K_{\alpha,JK} + S^\angle_\alpha, \tag{41}$$

where: α ($1 \leqslant \alpha \leqslant n_u$) is an index for the unrepresented species; J ($1 \leqslant J \leqslant n_r$) and K are indices for the represented species; $K_{\alpha,JK}$ is the manifold curvature (see Eqs. (25) and (B.7)); χ_{JK} is the scalar dissipation matrix of the represented species (Eq. (B.6)); $\mathbf{S}^\angle$ is the component of $\mathbf{S}$ in the unrepresented subspace (see Eq. (B.5) and Fig. 8); and the summation convention applies. Note the similarity between Eq. (41) and Eq. (9): the two terms on the right-hand sides are scalar dissipation times manifold curvature, and reaction. Note also that the CMC Equation (Eq. (35)) follows directly as the mean of Eq. (41) conditional on $\mathbf{y} = 0$.

A basic question which can be answered by Eq. (41) is the following [176]: in a turbulent reacting flow, if at time t_0 the compositions lie on the manifold (i.e., $\mathbf{y}(\mathbf{x},t_0) = 0$), do they remain on the manifold as the flow evolves? At time t_0, $\mathbf{y}$ is zero, so the left-hand side of Eq. (41) reduces to $\partial y_\alpha/\partial t$. Hence, the composition remains on the manifold only if this is zero, which requires that the right-hand side is zero. Now $K_{\alpha,JK}$ and $\mathbf{S}^\angle$ are non-random functions of $\mathbf{Y}^r$ (independent of the flow), whereas χ_{JK} is random and depends on the flow. Hence, for the right-hand side to be zero, it cannot be that the two terms balance (as is the case in a steady laminar flow): it must instead be that each term is zero. Given that χ_{JK} is random, the first term is zero only if the manifold is plane so that $K_{\alpha,JK}$ is zero. The reaction term $\mathbf{S}^\angle$ is zero only if the manifold is invariant, so that $\mathbf{S}$ is a tangent vector. For low-dimensional manifolds encountered in combustion, plane manifolds are not invariant, and invariant manifolds are not plane! This being the case, we conclude that (in turbulent combustion) compositions cannot lie exactly on a low-dimensional manifold: at best they may be close to a manifold.

Given that $\mathbf{y}$ is non-zero, the next question that can be asked is whether its complete neglect leading to Eq. (40) is a consistent approximation. The simple answer is "no" [187–189]. As discussed in Appendix B, a consistent analysis leads to the equation (for the I component of $\mathbf{S}^r$)

$$S^r_I = \widehat{S}^{r,m}_I + S^n_I + A_{IJK}\chi_{JK}, \tag{42}$$

where $\widehat{\mathbf{S}}^{r,m}$ is $\mathbf{S}^r$ evaluated on the manifold (Eq. (40)), and A_{IJK} is due to the curvature of the manifold (and is defined by Eq. (B.15)). In principle

the curvature term can be incorporated in the conservation equation for $\mathbf{Y}^r$, but in practice this would be very difficult, as it requires the evaluation (on the manifold) of the third-order tensor A_{IJK}, which is of size n_r^3. While manifold curvature is extremely important for very-low-dimensional manifolds, its importance inevitably decreases with manifold dimension. Hence, the neglect of the curvature term in Eq. (42) for QSSA and RCCE manifolds with $n_r \geqslant 10$, say, is likely not a significant source of error.

We refer to $\mathbf{S}^n$ (the second term on the right-hand side of Eq. (42)) as the *non-invariance correction*. This term (or a similar term) can and should be incorporated in the conservation equation for $\mathbf{Y}^r$, but it is usually neglected. Why this term arises and how it should be treated is well appreciated in some approaches [165,187–190] but not in others. In the hope of broadening its appreciation, this important issue is outlined and discussed in Section B.3.

6.4. The generation and tabulation of manifolds

In the generation of manifolds and the tabulation of their properties, there are two important distinctions to be made. The first is the distinction between *locally-generated* and *globally-generated* manifolds. In a locally-generated method, given a value of $\mathbf{Y}^r$ the corresponding manifold point $\mathbf{Y}^M(\mathbf{Y}^r)$ can be determined by a local calculation. Prime examples are QSSA, RCCE and ILDM. In contrast, globally-generated manifolds have to be constructed as a whole, usually as the solution of partial differential equations. Examples are SFM, FPV, FGM, FPI, REDIM and TGLDM. Because the whole of a globally-generated manifold has to be represented on a mesh, computational considerations limit the dimensionality to 2 or 3, seldom more.

The second distinction is between *structured pre-tabulation* and *in situ adaptive tabulation* (ISAT). The properties of globally-generated manifolds needed in a turbulent combustion calculation are generally pre-tabulated in a structured table. Because this is done prior to the turbulent combustion calculation, the whole space which could possibly be accessed must be tabulated. Again, computational considerations severely limit the dimensionality.

Using the method of *in situ* adaptive tabulation (ISAT) [83,191], a table of properties is built up during the turbulent combustion calculation, based on the compositions encountered. In this way, only the very small part of the species space which is accessed is tabulated; and, because of this, tabulations can be performed in much higher dimensions, e.g., 50D [76]. ISAT can be used in conjunction with not-too-large detailed and skeletal mechanisms (e.g., $n_r \leqslant 50$), and with locally-generated manifolds, notably QSSA and RCCE [135,159].

In general, pre-tabulation is used with globally-generated manifolds, and ISAT is used with locally-generated manifolds. However, pre-tabulation can also be used with very-low-dimensional, locally-generated manifolds.

To illustrate how ISAT works, we consider the task of tabulating the chemical source term $\mathbf{S} = \widehat{\mathbf{S}}(\mathbf{Y})$ based on the large number N of compositions $\mathbf{Y}^{(i)}$, $(1 \leqslant i \leqslant N)$ encountered sequentially in a turbulent combustion calculation. (In a typical LES/PDF calculation, N may be 10^{10} or larger.) The table built by ISAT consists of N_T table entries (e.g., $N_T = 10{,}000$), where the kth entry consists of: the location (in species space) of the point tabulated, $\mathbf{Y}^{[k]}$; the chemical source term, $\mathbf{S}^{[k]} = \widehat{\mathbf{S}}(\mathbf{Y}^{[k]})$; the Jacobian, $\mathbf{J}^{[k]} = \mathbf{J}(\mathbf{Y}^{[k]})$; and a hyper-ellipsoid $E^{[k]}$ centered at $\mathbf{Y}^{[k]}$. (Henceforth we refer to $E^{[k]}$ as an ellipsoid.) For given $\mathbf{Y}$, the linear approximation to $\mathbf{S}$ about $\mathbf{Y}^{[k]}$ is

$$\bar{\mathbf{S}}^{[k]}(\mathbf{Y}) \equiv \mathbf{S}^{[k]} + \mathbf{J}^{[k]}(\mathbf{Y} - \mathbf{Y}^{[k]}), \tag{43}$$

and the error in this approximation is

$$\epsilon^{[k]}(\mathbf{Y}) \equiv |\bar{\mathbf{S}}^{[k]}(\mathbf{Y}) - \widehat{\mathbf{S}}(\mathbf{Y})|. \tag{44}$$

The ellipsoid $E^{[k]}$ is such that the error $\epsilon^{[k]}(\mathbf{Y})$ is estimated to be less that the specified error tolerance ϵ_{tol} for every point $\mathbf{Y}$ in $E^{[k]}$.

The ISAT table is built up as the turbulent combustion computation proceeds in such a way that, with very high probability, every composition $\mathbf{Y}^{(i)}$ encountered is within some ellipsoid $E^{[k]}$, so that $\widehat{\mathbf{S}}(\mathbf{Y}^{(i)})$ can be approximated by $\bar{\mathbf{S}}^{[k]}(\mathbf{Y}^{(i)})$ with an error that is controlled by ϵ_{tol}. The ellipsoids are stored in various data structures, including binary trees, to facilitate searching for an ellipsoid $E^{[k]}$ which covers a given query point $\mathbf{Y}^{(i)}$. It may be observed that the union of the ellipsoids covers the empirical manifold.

In practice, ISAT is generally used, not to tabulate $\mathbf{S}$, but to tabulate the *reaction mapping*, which is defined as the solution to $d\mathbf{Y}/dt = \mathbf{S}$ at the end of the computational time step Δt, as a function of the initial condition. The current state of the art in using ISAT in LES/PDF computations is described in [134,135], including its combination with RCCE and its implementation on large parallel systems.

7. Discussion and conclusions

The ultimate goal in turbulent combustion modeling is to develop accurate, tractable and general predictive modeling capabilities. We have examined the challenges to be faced and some of the progress made in the past decade, focusing on non-premixed, gas-phase combustion.

The principal challenges are outlined in Section 3. The challenges of small scales and many species inevitably lead to statistical modeling of

the small-scale processes, and to a reduced description of the chemistry. Then the principal challenge is to account accurately and tractably for the coupled processes of reaction and molecular diffusion.

In the past decade, significant progress has been made on many fronts, especially in DNS, LES, PDF and in the development and reduction of chemical kinetics mechanisms for hydrocarbon fuels.

Computer power has reached the point where it is now possible to perform DNS under some (but not all) conditions of practical interest [3]. Such DNS are extremely valuable in the development and testing of turbulent combustion models. Nevertheless, for many decades to come, DNS will not be directly applicable in engineering applications of turbulent combustion because of the large range of scales involved—from those of the combustion chamber down to the smallest turbulent and reaction-zone scales. Because of this, a statistical approach is needed; either a completely statistical approach (as in RANS and PDF methods), or a statistical approach just for the small scales (as in LES and LES/PDF).

While RANS-based approaches remain prevalent in industry, LES is now prevalent in the research community and it will inevitably see increased use in industry. Since the processes of molecular mixing and reaction occur predominantly below the resolved scales, in LES, as in RANS, it is essential to account for the unresolved fluctuations and turbulence-chemistry interactions.

In the past decade, it has been convincingly demonstrated that PDF methods are capable of representing accurately the strong turbulence-chemistry interactions which occur in several laboratory jet flames [36,37]. This includes the significant local extinction and reignition in piloted jet flames [34,76], and the ignition and stabilization of lifted jet flames in vitiated co-flows [92,94].

Current chemical mechanisms for hydrocarbon fuels typically involve hundreds if not thousand of species—many more than can tractably be handled in a turbulent combustion model. Various reduction techniques based on the thermochemistry have been developed (see Sections 6.2.2 and 6.2.3) which for simple hydrocarbons can reduce the number of species (or other variables) needed to of order 20.

The current approaches to modeling non-premixed turbulent combustion have been reviewed, especially from the viewpoint of the implied manifolds in the species space. There is a clear dichotomy between flamelet-like approaches and PDF-like approaches, as described in Section 3.2. The principal characteristics of these two approaches are contrasted in Table 2.

Flamelet-like models are in general relatively simple to implement and inexpensive to use. However, they depend on the strong assumptions that the compositions occurring in turbulent combustion lie close to a very low-dimensional manifold, and that the coupling between turbulent mixing and reaction can be simply parameterized by at most one or two variables. While the limits of applicability and accuracy of such models are not easily delineated, it is certainly the case that they do not apply to the more challenging regimes of both non-premixed and premixed turbulent combustion, in which there is significant local extinction, or in which the turbulence significantly disrupts the reaction-diffusion balance of flamelet structures. This is clearly demonstrated in *a priori* testing (e.g., [178] and Fig. 11).

Table 2
Characteristics of flamelet-like and PDF-like models of turbulent combustion.

Characteristic	Flamelet-like models	PDF-like models
Examples and associated methods	Equilibrium, SFM, FPV, FGM, FPI, REDIM	PDF, MMC, LEM, ODT
Manifold assumption	Species lie on a very-low-dimensional manifold (e.g., 2D or 3D)	No assumption made (beyond that implied by the reduced chemistry employed)
Manifold properties	From laminar flame (or similar) calculations in pre-processing	Not applicable
Representation of composition in turbulent combustion calculation	Moments of Z (and in some cases C)	Joint PDF of species; represented by an ensemble of values of $\mathbf{Y}$
Treatment of complex chemistry	Confined to pre-processing	Exact, within turbulent combustion calculation
Tabulation	Structured tabulation in pre-processing (usually)	*in situ* adaptive tabulation, or none
Turbulent mixing to be modeled	Solely (or primarily) inert mixing	Reactive mixing
Treatment of coupling between reaction and molecular diffusion	Parameterized by few variables (e.g., χ)	Modeled implicitly by a mixing model (e.g., EMST, MMC); or ignored (e.g., IEM)
Determination of PDF	From a few moments and an assumed shape	From a modeled transport equation for the PDF

It is interesting to observe that all flamelet-like approaches lead to similar model equations, which reflect the assumed dominant balance between reaction and molecular diffusion, the latter represented as the product of scalar dissipation and manifold curvature: Eq. (9) in counter-flow flames and SFM; Eq. (16) in the equilibrium model; a generalization of Eq. (9) in REDIM; and also Eq. (35) in CMC (even though CMC is not a flamelet-like model). In turbulent combustion, for any very-low-dimensional manifold, there is an inevitable imbalance between reaction and molecular diffusion leading to departures from the manifold, as described by Eq. (41).

In the future we can expect to see further refinements to flamelet-like models, and their use in many applications. They may also form a useful component of an adaptive modeling strategy. The fact remains, however, that they are not applicable in the more challenging combustion regimes in which compositions do not lie close to very-low-dimensional manifolds, and in which the coupling between reaction and molecular diffusion cannot be simply parameterized.

PDF-like models (PDF, MMC, LEM, ODT) avoid the assumption of a very low-dimensional manifold, and hence have broader applicability. PDF and LES/PDF calculations have been reported with 53 and 38 species, respectively [76,134]. In these methods it is necessary to model the effects of molecular diffusion on reactive species. As discussed in Section 5.4, it is certainly the case that the simplest mixing models (e.g., IEM and MC) take no account of the effects of reaction on mixing. However, more sophisticated approaches (e.g., EMST and MMC) do account for these effects and there are good prospects for further improvements in such approaches.

PDF methods also provide a single framework which is applicable to all modes of combustion—non-premixed, premixed, partially-premixed—and, more generally, to systems with multiple inhomogeneous feed streams and with heat loss. For the next decade, a challenge for PDF models is to demonstrate the same success in premixed turbulent combustion as has been demonstrated in the past decade for non-premixed combustion, and to extend this success to spray flames and sooting flames.

A final comment is that, with the advent of accurate DNS in regimes of interest, turbulent combustion modeling can become less speculative! The assumptions made can be examined in detail using DNS data in both *a priori* and *a posteriori* testing. In particular, as illustrated in Section 6.2.7, it is possible to determine the dimensionality of plane and curved manifolds which adequately approximate the compositions occurring in different regimes of turbulent combustion; and mixing models can be subjected to both *a priori* and *a posteriori* testing.

Acknowledgments

I am grateful to Matthias Ihme for providing the data for Fig. 3, to Yue Yang for most of the results presented in Section 6.2.7, and to Varun Hiremath and Haifeng Wang for other contributions. For comments on the paper I am grateful to the reviewers and to Jackie Chen, Matt Cleary, Tarek Echekki, Tianfeng Lu, Ulrich Maas, Philip de Goey, Rob Gordon, Evatt Hawkes, Dan Haworth, Matthias Ihme, Alex Klimenko, Assaad Masri, Perrine Pepiot and James Sutherland. The research on dimension reduction of combustion chemistry is supported by Office of Energy Research, Office of Basic Energy Sciences, Chemical Sciences, Geosciences and Biosciences Division of the US Department of Energy (DOE) under Grant DE-FG02-90ER-14128. The research on PDF/LES and empirical manifolds is supported by the Combustion Energy Frontier Research Center, an Energy Frontier Research Center funded by the US Department of Energy, Office of Science, Office of Basic Energy Sciences under Award No. DE-SC0001198. The research on the efficient implementation of ethylene chemistry is supported by Grant No. FA9550-09-1-0611 funded by the National Center for Hypersonic Combined Cycle Propulsion, sponsored by the AFOSR and NASA ARMD.

Appendix A. Analysis of the EMST mixing model

For non-premixed combustion, it is shown that the EMST mixing model [90] (with simplifying assumptions) leads to an equation (Eq. (A.12)) for the species mass fractions which is similar to the unsteady flamelet model.

We consider a large number N of equal-mass computational particles, the ith of which has at time t mass fractions $\mathbf{Y}^i(t)$ and mixture fraction $Z_i(t)$. The analysis shows that the species mass fractions are given by

$$\mathbf{Y}^i(t) = \mathbf{Y}^E(Z_i(t), t), \tag{A.1}$$

where $\mathbf{Y}^E(z,t)$ evolves by Eq. (A.12). We take initial conditions such that the PDF of Z, $f(z)$, is self-similar (as explained below), and the species mass fractions are set by an appropriate specification of $\mathbf{Y}^E(z,0)$, e.g., corresponding to the steady flamelet model. This result is primarily of theoretical interest, as it provides a connection between PDF and flamelet modeling, and it shows that the molecular mixing of reactive species implied by the EMST model is appropriately affected by the chemical reactions.

It is convenient here to use an unconventional normalization of Z, such that its mean is zero. The particles are ordered in increasing mixture

fraction (i.e., $Z_i \geqslant Z_{i-1}$), so that the cumulative distribution function (CDF) of Z, $F(z)$, is such that

$$F(Z_i) = F_i \equiv i/N, \tag{A.2}$$

and an approximation to the PDF, $f(z)$, is provided by

$$\begin{aligned} 1 &= N[F(Z_{i+1}) - F(Z_i)] \\ &\approx N[Z_{i+1} - Z_i] f(Z_{i+1/2}), \end{aligned} \tag{A.3}$$

for $Z_{i+1/2} \equiv [Z_i + Z_{i+1}]/2$.

We do not consider the "intermittency" feature of the EMST model, so that all particles mix at all times. For the case considered, the EMST consists simply of edges between adjacent particles in the ordering. Consequently, according to the model [90], the particle mass fractions evolve by

$$\begin{aligned} \frac{d\mathbf{Y}^i}{dt} &= \gamma N^2 [w_{i-1/2}(\mathbf{Y}^{i-1} - \mathbf{Y}^i) + w_{i+1/2}(\mathbf{Y}^{i+1} - \mathbf{Y}^i)] \\ &\quad + \widehat{\mathbf{S}}(\mathbf{Y}^i), \end{aligned} \tag{A.4}$$

where

$$w_{i+1/2} \equiv 2\min(F_i, 1 - F_i), \tag{A.5}$$

and γ (determined below) controls the rate of mixing.

We assume that the PDF of Z, $f(z)$, decays in a self-similar manner. Consequently, we have

$$\frac{dZ_i}{dt} = -\omega Z_i, \tag{A.6}$$

where ω is the decay rate, which is related to the scalar dissipation by

$$\omega = \frac{1}{2}\langle\chi\rangle / \langle Z^2\rangle. \tag{A.7}$$

Thus, Eq. (A.4) written for Z_i and Eq. (A.6) yield

$$\begin{aligned} &-N^2[w_{i-1/2}(Z_{i-1} - Z_i) + w_{i+1/2}(Z_{i+1} - Z_i)] \\ &\quad = \frac{\omega}{\gamma} Z_i, \end{aligned} \tag{A.8}$$

or, in an obvious matrix notation,

$$\mathbf{A}\mathbf{Z} = \frac{\omega}{\gamma}\mathbf{Z}, \tag{A.9}$$

where $\mathbf{A}$ is the $N \times N$ sparse matrix defined by the left-hand side of Eq. (A.8). Evidently, $\mathbf{Z}$ is an eigenvector of $\mathbf{A}$ and ω/γ is the corresponding eigenvalue, denoted by λ. It is found numerically that as N increases, the relevant eigenvalue of $\mathbf{A}$ converges to $\lambda = 5.7832$, and that the standardized PDF, $f_o(z)$, of Z obtained from Eq. (A.3) converges to that shown in Fig. A.13. Thus γ is determined as $\gamma = \omega/\lambda$. The self-similar PDF is somewhat unusual and unphysical in that Z is bounded, and the PDF is discontinuous at the bounds.

Having determined the behavior of the mixture fraction, we return our attention to the species

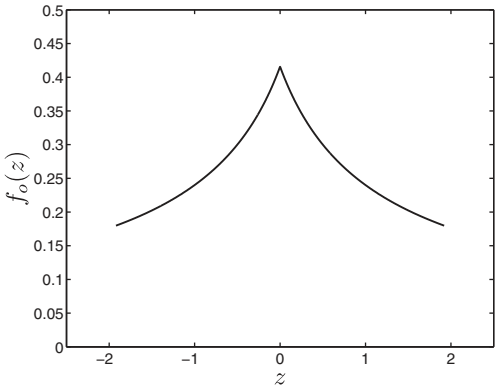

Fig. A.13. The standardized self-similar PDF of Z, $f_o(z)$.

mass fractions, which evolve by Eq. (A.4). We observe that, using Eq. (A.3), terms in this equation can be re-expressed as, for example,

$$N w_{i+1/2}(\mathbf{Y}^{i+1} - \mathbf{Y}^i) = \frac{w_{i+1/2}}{f_{i+1/2}} \frac{\mathbf{Y}^{i+1} - \mathbf{Y}^i}{Z_{i+1} - Z_i}. \tag{A.10}$$

In the limit as N tends to infinity, the divided difference becomes a derivative, and the right-hand side is written

$$\frac{w(z)}{f(z)} \frac{\partial \mathbf{Y}^E}{\partial z}. \tag{A.11}$$

Thus, in the limit as N tends to infinity, Eq. (A.4) becomes an evolution equation for $\mathbf{Y}^E(z,t)$:

$$\begin{aligned} \frac{\partial \mathbf{Y}^E}{\partial t} &= \frac{\gamma}{f}\frac{\partial}{\partial z}\left(\frac{w}{f}\frac{\partial \mathbf{Y}^E}{\partial z}\right) + \widehat{\mathbf{S}}(\mathbf{Y}^E) \\ &= \frac{1}{2}\langle\chi\rangle \frac{1}{f_o \lambda}\frac{\partial}{\partial z}\left(\frac{w}{f_o}\frac{\partial \mathbf{Y}^E}{\partial z}\right) + \widehat{\mathbf{S}}(\mathbf{Y}^E), \end{aligned} \tag{A.12}$$

where the second line follows from Eq. (A.7) and the relations $\gamma = \omega/\lambda$ and $f_o = f\langle Z^2\rangle^{1/2}$.

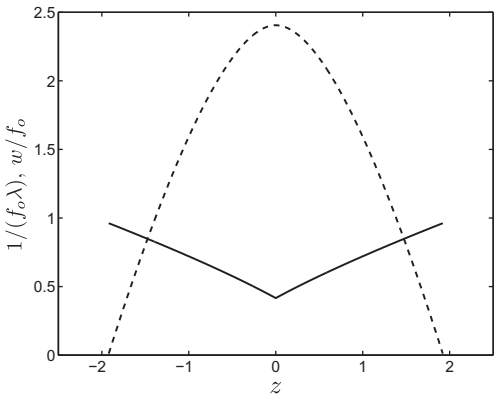

Fig. A.14. The coefficients $1/(f_o\lambda)$ (solid line) and w/f_o (dashed line) in Eq. (A.12).

As may be seen, Eq. (A.12) is similar to the unsteady flamelet equation. The non-dimensional, order-one coefficients $1/(f_o\,\lambda)$ and w/f_o are shown in Fig. A.14. Note that the mean $\langle\chi\rangle$, rather than instantaneous scalar dissipation χ, appears in Eq. (A.12): but there is no difficulty in extending the model by introducing a random process for $\gamma(t)$, leading to a model for $\chi(t)$ similar to the stochastic flamelet approach [192].

Appendix B. Conservation equations on manifolds

In Section B.1 we derive from Eq. (1) the conservation equation for the departure from the manifold, $\mathbf{y}$. Then, in Section B.2, an improved approximation for $\mathbf{S}^r$ is obtained. This includes the *non-invariance correction* $\mathbf{S}^n$, which is considered further in Section B.3. Similar analyses have previously been performed [176,188,189]: a difference here is that the manifold considered is parameterized by the represented species.

B.1. Conservation equation for the departure $\mathbf{y}$

For the manifold specified by $\mathbf{Y}^m(\mathbf{Y}^r)$, the departure $\mathbf{y}$ of the composition $\mathbf{Y}$ from the manifold is defined as

$$\mathbf{y} \equiv \mathbf{Y}^u - \mathbf{Y}^m(\mathbf{Y}^r). \tag{B.1}$$

Taking the material derivative of Eq. (B.1) we obtain

$$\frac{Dy_\alpha}{Dt} = \frac{DY^u_\alpha}{Dt} - T^u_{\alpha,I}\frac{DY^r_I}{Dt}, \tag{B.2}$$

where

$$T^u_{\alpha,I} \equiv \frac{\partial Y^m_\alpha}{\partial Y^r_I}, \tag{B.3}$$

represents the components of the tangent vectors in the unrepresented subspace. We use lowercase Greek letters for indices of unrepresented quantities (e.g., $1 \leqslant \alpha \leqslant n_u$), and upper-case Roman letters for represented quantities (e.g., $1 \leqslant I \leqslant n_r$).

Expressions for DY^u_α/Dt and DY^r_I/Dt are obtained simply from Eq. (1). Substituting these into Eq. (B.2), after manipulation we obtain

$$\frac{Dy_\alpha}{Dt} = \frac{1}{\rho}\nabla\cdot(\rho D\nabla y_\alpha) + S^\angle_\alpha + \chi_{JK}K_{\alpha,JK}, \tag{B.4}$$

where:

$$S^\angle_\alpha \equiv S^u_\alpha - T^u_{\alpha I}S^r_I, \tag{B.5}$$

is the component of $\mathbf{S}$ in the unrepresented subspace not in the tangent space (see Fig. 8);

$$\chi_{JK} \equiv D\nabla Y^r_J\cdot\nabla Y^r_K, \tag{B.6}$$

is the scalar-dissipation matrix of the represented species; and

$$K_{\alpha,JK} \equiv \frac{\partial^2 Y^m_\alpha}{\partial Y^r_J \partial Y^r_K}, \tag{B.7}$$

is the manifold curvature.

B.2. Improved approximation for the represented chemical source term $\mathbf{S}^r$

We now perform an analysis (similar to that of [176,188,189]) for the case in which $\mathbf{y}$ is sufficiently small that it can be neglected everywhere except in the chemical source term $\mathbf{S}$, and that the dependence of $\mathbf{S}$ on $\mathbf{y}$ can be linearized. Subject to these conditions, Eq. (B.4) becomes

$$0 = S^{\angle m}_\alpha + J^{\angle u}_{\alpha\beta}y_\beta + \chi_{JK}K_{\alpha,JK}, \tag{B.8}$$

where $\mathbf{S}^{\angle m}$ denotes $\mathbf{S}^\angle$ evaluated on the manifold, and

$$J^{\angle u}_{\alpha\beta} \equiv \frac{\partial S^\angle_\alpha}{\partial Y^u_\beta}, \tag{B.9}$$

is also evaluated on the manifold. We assume that the manifold is attracting, so that all of the eigenvalues of the $n_u \times n_u$ matrix $\mathbf{J}^{\angle u}$ have strictly negative real part, and therefore $\mathbf{J}^{\angle u}$ possesses an inverse, whose components are denoted by $J^{\angle u-1}_{\alpha\beta}$. Then, $\mathbf{y}$ is uniquely determined by Eq. (B.8) as

$$y_\gamma = -J^{\angle u-1}_{\gamma\alpha}(S^{\angle m}_\alpha + \chi_{JK}K_{\alpha,JK}). \tag{B.10}$$

This solution yields the value of $\mathbf{y}$ (and hence of $\mathbf{Y}$) such that, in the unrepresented subspace, the chemical source term exactly balances the dissipation-curvature.

In place of Eq. (40), the improved, linear approximation for $\mathbf{S}^r$ is

$$S^r_I = \widehat{S}^{r,m}_I + J^{ru}_{I\gamma}y_\gamma, \tag{B.11}$$

where $\mathbf{J}^{ru}$ is defined by

$$J^{ru}_{I\gamma} \equiv \frac{\partial S^r_I}{\partial Y^u_\gamma}. \tag{B.12}$$

Using Eq. (B.10) for y_γ, we obtain

$$S^r_I = \widehat{S}^{r,m}_I + S^n_I + A_{IJK}\chi_{JK}, \tag{B.13}$$

where $\mathbf{S}^n$, which is due to the non-invariance of the manifold, is

$$S^n_I \equiv -J^{ru}_{I\gamma}J^{\angle u-1}_{\gamma\alpha}S^{\angle m}_\alpha, \tag{B.14}$$

and we define

$$A_{IJK} \equiv -J^{ru}_{I\gamma}J^{\angle u-1}_{\gamma\alpha}K_{\alpha,JK}. \tag{B.15}$$

Note that $\mathbf{J}^{ru}$ and $\mathbf{J}^{\angle u}$ represent different parts of the Jacobian (Eq. (8)) and have dimensions of inverse time. There is no apparent reason why the non-dimensional product $\mathbf{J}^{ru}\mathbf{J}^{\angle u-1}$ should in general be small, and hence that the final terms in Eq. (B.13) should be negligibly small. Indeed, exam-

ples are readily constructed [189] in which these final terms have a significant effect.

B.3. The non-invariance correction

We now examine in more detail the additional term $\mathbf{S}^n$ which arises due to the non-invariance of the manifold. We refer to this as the *non-invariance correction*.

For the simplest case of a homogeneous mixture, Eq. (1) becomes

$$\frac{d}{dt}\begin{bmatrix}\mathbf{Y}^r\\ \mathbf{Y}^u\end{bmatrix} = \begin{bmatrix}\mathbf{S}^r\\ \mathbf{S}^u\end{bmatrix} = \begin{bmatrix}\widehat{\mathbf{S}}^r(\mathbf{Y})\\ \widehat{\mathbf{S}}^u(\mathbf{Y})\end{bmatrix}. \tag{B.16}$$

With the assumption that the composition $\mathbf{Y}$ is on the manifold, it appears to follow trivially that $\mathbf{Y}^r$ evolves by

$$\frac{d\mathbf{Y}^r}{dt} = \widehat{\mathbf{S}}^{r,m} \equiv \widehat{\mathbf{S}}^r(\mathbf{Y}^M(\mathbf{Y}^r)). \tag{B.17}$$

However, even for a plane manifold, there is a logical flaw in the argument, namely that it is based on inconsistent premises. Specifically, the assumption $\mathbf{Y}(t) = \mathbf{Y}^M(\mathbf{Y}^r(t))$ implies that the rate of change of $\mathbf{Y}$ is in the tangent space, since the chain rule yields

$$\frac{dY_i}{dt} = T_{iJ}\frac{dY^r_J}{dt}, \tag{B.18}$$

where $T_{iJ} \equiv \partial Y^M_i/\partial Y^r_J$ is the i-component of the Jth tangent vector. However, in general, Eq. (B.16) is inconsistent with Eq. (B.18). It is consistent only if the manifold is invariant or, equivalently, if $\mathbf{S}^\angle$ is zero.

There are two ways to remove the inconsistency. The first way is that used above in Section B.2, which has been termed the *close-parallel* assumption [188]. According to this assumption, there is an invariant manifold close to and parallel to the specified manifold $\mathbf{Y} = \mathbf{Y}^M(\mathbf{Y}^r)$. The chemical source term is evaluated on this invariant manifold, and it is entirely in the tangent space (i.e., $\mathbf{S}^\angle = 0$) because, by the "parallel" assumption, the two manifolds share the same tangent space.

The second way is to replace $\mathbf{S}$ (evaluated on the manifold) by a projection of $\mathbf{S}$ onto the tangent space. We denote this projection by

$$\mathbf{S}^p = \mathbf{P}\mathbf{S}, \tag{B.19}$$

where $\mathbf{P}$ is an $n_s \times n_s$ projection matrix. But what projection to use? Some possibilities, illustrated in Fig. B.15, are:

1. Project in the unrepresented subspace, which yields $\mathbf{S}^r = \widehat{\mathbf{S}}^{r,m}$, i.e., $\mathbf{S}^n = 0$.
2. Project in the normal subspace.
3. Project in the "fast" subspace.
4. Use a projector based on thermodynamics [190].

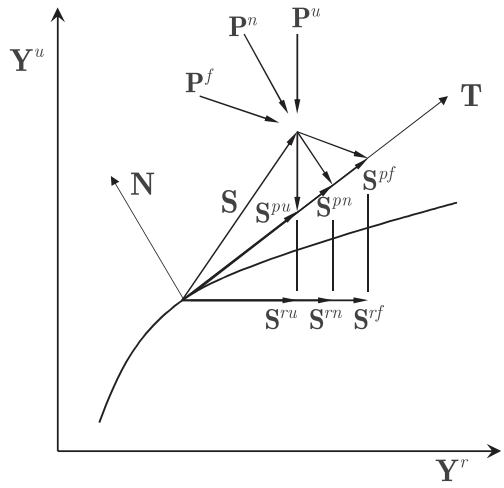

Fig. B.15. Sketch showing a 1D manifold, the chemical source term $\mathbf{S}$ and its projections ($\mathbf{S}^{pu}$, $\mathbf{S}^{pn}$ and $\mathbf{S}^{pf}$) onto the tangent space using different projectors ($\mathbf{P}^u$, $\mathbf{P}^n$ and $\mathbf{P}^f$ in the unrepresented, normal and fast subspaces). This illustrates that different projectors lead to different rates of change of the represented species ($\mathbf{S}^{ru}$, $\mathbf{S}^{rn}$ and $\mathbf{S}^{rf}$).

It should be recognized that projections (1) and (2) contain arbitrariness and lack rational support. The same manifold can be parameterized by different represented species, and when this is done projection (1) yields different results. The definition of the normal subspace depends on the scaling of the variables. Different results are obtained if the species are represented in specific moles instead of mass fractions. For a PCA manifold, the normal subspace depends on how the scaling in the PCA is performed.

In contrast to projections (1) and (2), based on an analysis of Eq. (B.16), both the CSP and ILDM methods identify the appropriate projector in the "fast" subspace [165,166]. The result is very similar to the projection implied by the close parallel analysis which leads to $\mathbf{S}^n$ given by Eq. (B.14). The importance of using the correct projector is illustrated in [187,189].

References

[1] N. Peters, *Proc. Combust. Inst.* 32 (2009) 1–25.
[2] K.N.C. Bray, *Proc. Combust. Inst.* 26 (1996) 1–26.
[3] J.H. Chen, *Proc. Combust. Inst.* 33 (2011) 99–123.
[4] R.S. Barlow, *Proc. Combust. Inst.* 31 (2007) 49–75.
[5] R.W. Bilger, S.B. Pope, K.N.C. Bray, J.F. Driscoll, *Proc. Combust. Inst.* 30 (2005) 21–42.
[6] T. Takeno, *Proc. Combust. Inst.* 25 (1994) 1061–1073.
[7] D. Bradley, *Proc. Combust. Inst.* 24 (1992) 247–262.
[8] S.B. Pope, *Proc. Combust. Inst.* 23 (1990) 591–612.

[9] R.W. Bilger, *Proc. Combust. Inst.* 22 (1988) 475–488.
[10] N. Peters, *Proc. Combust. Inst.* 21 (1986) 1231–1250.
[11] A. McIlroy, G. McRae, *Basic Research Needs for Clean and Efficient Combustion of 21st Century Transportation Fuels*, US Department of Energy, Basic Energy Sciences, 2007, available at http://www.sc.doe.gov/bes/reports/files/CTF_rpt.pdf.
[12] M. Boileau, G. Staffelbach, B. Cuenot, T. Poinsot, C. Berat, *Combust. Flame* 154 (2008) 2–22.
[13] F.A. Williams, *Combustion Theory*, Benjamin, Cummings, Menlo Park, 1985.
[14] S.B. Pope, *Turbulent Flows*, Cambridge University Press, Cambridge, 2000.
[15] T. Poinsot, D. Veynante, in: T. Poinsot, D. Veynante (Eds.), *Theoretical and Numerical Combustion*, third ed. Toulouse, 2011.
[16] C.K. Law, *Proc. Combust. Inst.* 31 (2007) 1–29.
[17] L.F. Shampine, I. Gladwell, S. Thompson, *Solving ODEs with MATLAB*, Cambridge University Press, 2003.
[18] J. Bell, M. Day, in: T. Echekki, E. Mastorakos (Eds.), *Turbulent Combustion*. Springer, 2011, pp. 301–329.
[19] D.A. Schwer, P.S. Lu, W.H. Green, *Combust. Flame* 133 (2003) 451–465.
[20] I. Banerjee, M. Ierapetritou, *Combust. Flame* 144 (2006) 619–633.
[21] Y. Shi, R.P. Hessel, R.D. Reitz, *Combust. Theor. Model.* 13 (2009) 83–104.
[22] L. Liang, J. Stevens, J. Farrel, *Proc. Combust. Inst.* 32 (2009) 527–534.
[23] F. Contino, H. Jeanmart, T. Lucchini, G. D'Errico, *Proc. Combust. Inst.* 33 (2011) 3057–3064.
[24] T. Løvas, S. Navarro-Martinez, S. Rigopoulos, *Proc. Combust. Inst.* 33 (2011) 1339–1346.
[25] F.R. Menter, Y. Egorov, *Flow Turbul. Combust.* 85 (2010) 113–138.
[26] S. Jakirlic, G. Kadavelila, M. Kornhaasa, M. Schfera, D.C. Sternela, C. Tropea, *Int. J. Heat Fluid Flow* 31 (2010) 820–832.
[27] S.B. Pope, *Phys. Fluids* 23 (2011) 011301.
[28] C.K. Law, *Combustion Physics*, Cambridge University Press, New York, 2006.
[29] R.J. Kee, M.E. Coltrin, P. Glarborg, *Chemically reacting flow: theory and practice*, Wiley, Hoboken, 2003.
[30] T. Lu, C.K. Law, *Combust. Flame* 144 (2006) 24–36.
[31] C.J. Sung, C.K. Law, J.-Y. Chen, *Proc. Combust. Inst.* 27 (1998) 295–304.
[32] G.E. Esposito, H.K. Chelliah, *Combust. Flame* 158 (2011) 477–489.
[33] T. Echekki, E. Mastorakos, in: T. Echekki, E. Mastorakos (Eds.), *Turbulent Combustion*, Springer, 2011, pp. 19–39.
[34] R.S. Barlow, J.H. Frank, *Proc. Combust. Inst.* 27 (1998) 1087–1095.
[35] S.B. Pope, *Prog. Energy Combust. Sci.* 11 (1985) 119–192.
[36] D.C. Haworth, *Prog. Energy Combust. Sci.* 36 (2010) 168–259.
[37] D.C. Haworth, S.B. Pope, in: T. Echekki, E. Mastorakos (Eds.), *Turbulent Combustion*. Springer, 2011, pp. 119–142.
[38] K.A. Kemenov, S.B. Pope, *Combust. Flame* 157 (2011) 240–254.
[39] J.H. Frank, S.A. Kaiser, *Exp. Fluids* 49 (2010) 823–837.
[40] Z. Warhaft, *Annu. Rev. Fluid. Mech.* 32 (2000) 203–240.
[41] M. Matalon, *Proc. Combust. Inst.* 32 (2009) 57–82.
[42] T. Echekki, E. Mastorakos, *Turbulent Combustion Modeling*, Springer, 2011.
[43] N. Peters, *Prog. Energy Combust. Sci.* 10 (1984) 319–339.
[44] N. Peters, *Turbulent Combustion*, Cambridge University Press, 2000.
[45] C.D. Pierce, P. Moin, *J. Fluid Mech.* 504 (2004) 73–97.
[46] M. Ihme, H. Pitsch, *Combust. Flame* 155 (2008) 70–89.
[47] M. Ihme, H. Pitsch, *Combust. Flame* 155 (2008) 90–107.
[48] J.A. van Oijen, L.P.H. de Goey, *Combust. Sci. Technol.* 161 (2000) 113–138.
[49] O. Gicquel, N. Darabiha, D. Thévenin, *Proc. Combust. Inst.* 28 (2000) 1901–1908.
[50] V. Bykov, U. Maas, *Combust. Theor. Model.* 11 (2007) 839–862.
[51] V. Bykov, U. Maas, *Proc. Combust. Inst.* 32 (2009) 561–568.
[52] D.C. Haworth, M.C. Drake, S.B. Pope, R.J. Blint, *Proc. Combust. Inst.* 21 (1989) 589–597.
[53] H. Pitsch, M. Chen, N. Peters, *Proc. Combust. Inst.* 27 (1998) 1057–1064.
[54] A.Y. Klimenko, S.B. Pope, *Phys. Fluids* 15 (2003) 1907–1925.
[55] M.J. Cleary, A.Y. Klimenko, in: T. Echekki, E. Mastorakos (Eds.), *Turbulent Combustion Modeling*. Springer, 2011, pp. 143–173.
[56] A.R. Kerstein, *Combust. Sci. Technol.* 60 (1988) 391–421.
[57] S. Menon, A.R. Kerstein, in: T. Echekki, E. Mastorakos (Eds.), *Turbulent Combustion*. Springer, 2011, pp. 221–247.
[58] A.R. Kerstein, *J. Fluid Mech.* 392 (1999) 277–334.
[59] T. Echekki, A.R. Kerstein, J.C. Sutherland, in: T. Echekki, E. Mastorakos (Eds.), *Turbulent Combustion*. Springer, 2011, pp. 249–276.
[60] R.W. Bilger, *Phys. Fluids A* 5 (1993) 436–444.
[61] A.Y. Klimenko, R.W. Bilger, *Prog. Energy Combust. Sci.* 25 (1999) 595–687.
[62] A. Kronenburg, E. Mastorakos, in: T. Echekki, E. Mastorakos (Eds.), *Turbulent Combustion Modeling*. Springer, 2011, pp. 91–117.
[63] B.F. Magnussen, B.H. Mjertager, *Proc. Combust. Inst.* 16 (1976) 719–727.
[64] W.R. Hawthorne, D.S. Weddell, H.C. Hottel, *Proc. Combust. Inst.* 3 (1949) 254–300.
[65] J.H. Kent, R.W. Bilger, *Proc. Combust. Inst.* 14 (1973) 615–625.
[66] R.W. Bilger, *Combust. Sci. Technol.* 13 (1976) 155–170.
[67] P.K. Yeung, *Phys. Fluids* 10 (1998) 2621–2635.
[68] L. Mydlarski, Z. Warhaft, *J. Fluid Mech.* 358 (1998) 135–175.
[69] A. Gylfason, Z. Warhaft, *Phys. Fluids* 16 (2004) 4012–4019.
[70] B. Cuenot, in: T. Echekki, E. Mastorakos (Eds.), *Turbulent Combustion*. Springer, 2011, pp. 43–61.
[71] M. Ihme, Y.C. See, *Combust. Flame* 157 (2010) 1850–1862.
[72] M. Ihme, H. Pitsch, *Phys. Fluids* 20 (2008) 055110.

[73] M. Ihme, Y.C. See, *Proc. Combust. Inst.* 33 (2011) 1309–1317.
[74] R.O. Fox, *Computational Models for Turbulent Reactive Flows*, Cambridge University Press, New York, 2003.
[75] P. Givi, *AIAA J.* 44 (2006) 16–23.
[76] R. Cao, S.B. Pope, *Combust. Flame* 143 (2005) 450–470.
[77] G.P. Smith, D.M. Golden, M. Frenklach, et al., GRI-Mech 3.0, 2003, available at http://www.me.berkeley.edu/gri_mech.
[78] R.S. Mehta, M.F. Modest, D.C. Haworth, *Combust. Theor. Model.* 14 (2010) 105–124.
[79] M. Muradoglu, P. Jenny, S.B. Pope, D.A. Caughey, *J. Comput. Phys.* 154 (1999) 342–371.
[80] L. Valino, *Flow Turbul. Combust.* 60 (1998) 157–172.
[81] P.J. Colucci, F.A. Jaberi, P. Givi, S.B. Pope, *Phys. Fluids* 10 (1998) 499–515.
[82] V. Raman, H. Pitsch, *Proc. Combust. Inst.* 31 (2007) 1711–1719.
[83] S.B. Pope, *Combust. Theor. Model.* 1 (1997) 41–63.
[84] S.B. Pope, *J. Fluid Mech.* 652 (2010) 139–169.
[85] S.H. Starner, R.W. Bilger, *Combust. Flame* 61 (1985) 29–38.
[86] A.R. Masri, R.W. Bilger, *Proc. Combust. Inst.* 21 (1986) 1511–1520.
[87] J. Xu, S.B. Pope, *Combust. Flame* 123 (2000) 281–307.
[88] Q. Tang, J. Xu, S.B. Pope, *Proc. Combust. Inst.* 28 (2000) 133–139.
[89] R.P. Lindstedt, S.A. Louloudi, E.M. Váos, *Proc. Combust. Inst.* 28 (2000) 149–156.
[90] S. Subramaniam, S.B. Pope, *Combust. Flame* 115 (1998) 487–514.
[91] R.R. Cao, H. Wang, S.B. Pope, *Proc. Combust. Inst.* 31 (2007) 1543–1550.
[92] R. Cabra, T. Myhrvold, J.Y. Chen, R.W. Dibble, A.N. Karpetis, R.S. Barlow, *Proc. Combust. Inst.* 29 (2002) 1881–1888.
[93] A.R. Masri, R. Cao, S.B. Pope, G.M. Goldin, *Combust. Theor. Model.* 8 (2004) 1–22.
[94] R. Cao, S.B. Pope, A.R. Masri, *Combust. Flame* 142 (2005) 438–453.
[95] R.L. Gordon, A.R. Masri, S.B. Pope, G.M. Goldin, *Combust. Theor. Model.* 11 (2007) 351–376.
[96] R.L. Gordon, A.R. Masri, S.B. Pope, G.M. Goldin, *Combust. Flame* 151 (2007) 495–511.
[97] H. Wang, S.B. Pope, *Combust. Theor. Model.* 12 (2008) 857–882.
[98] C. Duwig, L. Fuchs, *Combust. Sci. Technol.* 180 (2008) 453–480.
[99] S. Navarro-Martinez, S. Rigopoulos, *Flow Turbul. Combust.* 87 (2011) 407–423.
[100] T. Myhrvold, I.R. Gran, R. Cabra, J.-Y. Chen, *Combust. Sci. Technol.* 178 (2006) 1001–1030.
[101] S. Navarro-Martinez, A. Kronenburg, *Flow Turbul. Combust.* 87 (2011) 377–406.
[102] C.S. Yoo, R. Sankaran, J.H. Chen, *J. Fluid Mech.* 460 (2009) 453–481.
[103] Z. Wu, S.H. Starner, R.W. Bilger, in: D. Honnery (Ed.), Proceedings of the 2003 Australian Symposium on Combustion and the Eighth Australian Flame Days, The Combustion Institute, 2003.
[104] J. Villermaux, J.C. Devillon, *in: Proceedings of the Second International Symposium on Chemical Reaction Engineering*, Elsevier, New York, 1972, pp. 1–13.
[105] C. Dopazo, E.E. O'Brien, *Acta Astronaut.* 1 (1974) 1239–1266.
[106] R.L. Curl, *AIChE J.* 9 (1963) 175–181.
[107] J. Janicka, W. Kolbe, W. Kollmann, *J. Non-Equilib. Thermodyn* 4 (1977) 47–66.
[108] P.A. Nooren, H.A. Wouters, T.W.J. Peeters, D. Roekaerts, U. Maas, D. Schmidt, *Combust. Theor. Model.* 1 (1997) 79–96.
[109] S.B. Pope, M.S. Anand, *Proc. Combust. Inst.* 20 (1985) 403–410.
[110] M.S. Anand, S.B. Pope, *Combust. Flame* 67 (1987) 127–142.
[111] A.T. Norris, S.B. Pope, *Combust. Flame* 83 (1990) 27–42.
[112] E.R. Hawkes, R. Sankaran, J.C. Sutherland, J.H. Chen, *Proc. Combust. Inst.* 31 (2007) 1633–1640.
[113] E.S. Richardson, R. Sankaran, R.W. Grout, J.H. Chen, *Combust. Flame* 157 (2010) 506–515.
[114] E.S. Richardson, J.H. Chen, *Combust. Flame* 159, submitted for publication.
[115] R.P. Lindstedt, E.M. Váos, *Combust. Flame* 145 (2006) 495–511.
[116] P. Givi, *Prog. Energy Combust. Sci.* 15 (1989) 1–107.
[117] F. Gao, E.E. O'Brien, *Phys. Fluids A* 5 (1993) 1282–1284.
[118] F.A. Jaberi, P.J. Colucci, S. James, P. Givi, S.B. Pope, *J. Fluid Mech.* 401 (1999) 85–121.
[119] L.Y.M. Gicquel, P. Givi, F.A. Jaberi, S.B. Pope, *Phys. Fluids* 14 (2002) 1196–1213.
[120] M.R.H. Sheikhi, T.G. Drozda, P. Givi, S.B. Pope, *Phys. Fluids* 15 (2003) 2321–2337.
[121] M.R.H. Sheikhi, T.G. Drozda, P. Givi, F.A. Jaberi, S.B. Pope, *Proc. Combust. Inst.* 30 (2005) 549–556.
[122] M.R.H. Sheikhi, P. Givi, S.B. Pope, *Phys. Fluids* 19 (2007) 095106.
[123] M.R.H. Sheikhi, P. Givi, S.B. Pope, *Phys. Fluids* 21 (2009) 075102.
[124] M.B. Nik, S.L. Yilmaz, P. Givi, M.R.H. Sheikhi, S.B. Pope, *AIAA J.* 48 (2010) 1513–1522.
[125] S. James, J. Zhu, M.S. Anand, *Proc. Combust. Inst.* 31 (2007) 1737–1745.
[126] A.J. Chandy, D.J. Glaze, S.H. Frankel, *J. Heat Trans.* 131 (2009) 051201.
[127] H. Wang, S.B. Pope, *Proc. Combust. Inst.* 33 (2011) 1319–1330.
[128] W.P. Jones, V.N. Prasad, *Combust. Flame* 157 (2010) 1621–1636.
[129] V.A. Sabel'nikov, O. Soulard, *Phys. Rev. E* 72 (2005) 016,30.
[130] Y. Yang, H. Wang, S.B. Pope, J.H. Chen, *Proc. Combust. Inst*. (2012), http://dx.doi.org/10.1016/j.proci.2012.08.015.
[131] R. McDermott, S.B. Pope, *J. Comput. Phys.* 226 (2007) 947–993.
[132] S. Viswanathan, H. Wang, S.B. Pope, *J. Comput. Phys.* 230 (2011) 6916–6957.
[133] E. Knudsen, E.S. Richardson, E.M. Doran, H. Pitsch, J.H. Chen, *Phys. Fluids* 24 (2012) 055103.
[134] V. Hiremath, S.R. Lantz, H. Wang, S.B. Pope, *Combust. Flame* 159 (2012) 3096–3109.
[135] V. Hiremath, S.R. Lantz, H. Wang, S.B. Pope, *Proc. Combust. Inst.* (2012), http://dx.doi.org/10.1016/j.proci.2012.06.004.

[136] A.P. Wandel, A.Y. Klimenko, *Phys. Fluids* 17 (2005) 128105.
[137] M.J. Cleary, A. Kronenburg, *Proc. Combust. Inst.* 31 (2007) 1497–1505.
[138] A.P. Wandel, R.P. Lindstedt, *Phys. Fluids* 21 (2009) 015103.
[139] M.J. Cleary, A.Y. Klimenko, J. Janicka, M. Pfitzner, *Proc. Combust. Inst.* 32 (2009) 1499–1507.
[140] M.J. Cleary, A.Y. Klimenko, *Flow Turbul. Combust.* 82 (2009) 477–491.
[141] K. Vogiatzaki, M.J. Cleary, A. Kronenburg, J.H. Kent, *Phys. Fluids* 21 (2009) 025105.
[142] H. El-Asrag, S. Menon, *Proc. Combust. Inst.* 31 (2007) 1747–1754.
[143] B.A. Sen, S. Menon, *Combust. Flame* 157 (2010) 62–74.
[144] B. Ranganath, T. Echekki, *Combust. Sci. Technol.* 181 (2009) 570–596.
[145] N. Punati, J.C. Sutherland, A.R. Kerstein, E.R. Hawkes, J.H. Chen, *Proc. Combust. Inst.* 33 (2011) 1515–1522.
[146] J. Park, T. Echekki, *Combust. Flame* 159 (2012) 609–620.
[147] D.O. Lignell, D.S. Rappleye, *Combust. Flame* 159 (2012) 2930–2943.
[148] T. Lu, C.K. Law, *Proc. Combust. Inst.* 30 (2005) 1333–1341.
[149] P. Pepiot, H. Pitsch, *Combust. Flame* 154 (2008) 67–81.
[150] K.E. Niemeyer, C.-J. Sung, M.P. Raju, *Combust. Flame* 157 (2010) 1760–1770.
[151] H. Wang, M. Frenklach, *Combust. Flame* 87 (1991) 365–370.
[152] B. Bhattacharjee, D. Schwer, P. Barton, W. Green, *Combust. Flame* 135 (2003) 191–208.
[153] J. Luche, M. Reuillon, J.-C. Boettner, M. Cathonnet, *Combust. Sci. Technol.* 176 (2004) 1935–1963.
[154] M. Valorani, F. Creta, D. Goussis, J. Lee, H. Najm, *Combust. Flame* 146 (2006) 29–51.
[155] T. Nagy, T. Turanyi, *Combust. Flame* 156 (2009) 417–428.
[156] J.C. Keck, D. Gillespie, *Combust. Flame* 17 (1971) 237.
[157] D. Hamiroune, P. Bishnu, M. Metghalchi, J.C. Keck, *Combust. Theor. Model.* 2 (1998) 81–94.
[158] Z. Ren, G.M. Goldin, V. Hiremath, S.B. Pope, *Combust. Theor. Model.* 15 (2011) 827–848.
[159] V. Hiremath, Z. Ren, S.B. Pope, *Combust. Flame* 158 (2010) 2113–2127.
[160] W.P. Jones, S. Rigopoulos, *Combust. Flame* 142 (2005) 223–234.
[161] W.P. Jones, S. Rigopoulos, *Combust. Theor. Model.* 11 (2007) 755–780.
[162] V. Hiremath, Z. Ren, S.B. Pope, *Combust. Theor. Model.* 14 (2010) 619–652.
[163] S.B. Pope, U. Maas, Simplifying Chemical Kinetics: Trajectory-Generated Low-Dimensional Manifolds, FDA 93-11, Cornell University, 1993.
[164] M. Bodenstein, S.C. Lind, *Z. Phys. Chem.* 57 (1906) 168.
[165] U.A. Maas, S.B. Pope, *Combust. Flame* 88 (1992) 239–264.
[166] S.H. Lam, D.A. Goussis, *Int. J. Chem. Kinet.* 26 (1994) 461–486.
[167] Z. Ren, S.B. Pope, A. Vladimirsky, J.M. Guckenheimer, *J. Chem. Phys.* 124 (2006) 114111.
[168] Z. Ren, S.B. Pope, A. Vladimirsky, J.M. Guckenheimer, *Proc. Combust. Inst.* 31 (2007) 473–481.
[169] M.D. Smooke (Ed.), Reduced kinetic mechanisms and asymptotic approximations for methane–air flames, Volume 384 of Lecture Notes in Physics. Springer, Berlin, 1991.
[170] N. Peters, B. Rogg (Eds.), *Reduced Kinetic Mechanisms for Applications in Combustion Systems*, Springer, Berlin, 1993.
[171] T. Lu, C.K. Law, *Prog. Energy Combust. Sci.* 35 (2009) 192–215.
[172] T. Lu, C.K. Law, *J. Phys. Chem. A* 110 (2006) 13202–13208.
[173] B.J. Debusschere, Y.M. Marzouk, H.N. Najm, B. Rhoads, D.A. Goussis, M. Valorani, *Combust. Theor. Model.* 16 (2012) 173–198.
[174] T.F. Lu, C.K. Law, *Combust. Flame* 154 (2008) 761–774.
[175] T. Løvas, F. Mauss, C. Hasse, N. Peters, *Proc. Combust. Inst.* 29 (2002) 1403–1410.
[176] S.B. Pope, *Flow Turbul. Combust.* 72 (2004) 219–243.
[177] H. Bongers, J.A. Van Oijen, L.P.H. de Goey, *Proc. Combust. Inst.* 29 (2003) 1371–1378.
[178] J.C. Sutherland, A. Parente, *Proc. Combust. Inst.* 32 (2009) 1563–1570.
[179] A. Parente, J.C. Sutherland, L. Tognotti, P.J. Smith, *Proc. Combust. Inst.* 32 (2009) 1579–1586.
[180] A. Parente, J.C. Sutherland, B.B. Dally, L. Tognotti, P.J. Smith, *Proc. Combust. Inst.* 33 (2011) 3333–3341.
[181] A. Biglari, J.C. Sutherland, *Combust. Flame* 159 (2012) 1960–1970.
[182] Y. Yang, S.B. Pope, *Combust. Theor. Model.* 16, in preparation.
[183] C.S. Yoo, E.S. Richardson, R. Sankaran, J.H. Chen, *Proc. Combust. Inst.* 33 (2011) 1619–1627.
[184] J.H. Friedman, C.B. Roosen, *Stat. Meth. Med. Res.* 4 (1995) 197–217.
[185] J.B. Tenenbaum, V. de Silva, J.C. Langford, *Science* 22 (2000) 2319–2323.
[186] G. Bansal, A. Mascarenhas, J.H. Chen, in: Seventh US National Meeting of the Combustion Institute, Georgia Institute of Technology, Atlanta, GA, 2011.
[187] S.H. Lam, *Combust. Sci. Technol.* 179 (2007) 767–786.
[188] Q. Tang, S.B. Pope, *Proc. Combust. Inst.* 29 (2002) 1411–1417.
[189] Z. Ren, S.B. Pope, *Combust. Theor. Model.* 11 (2007) 715–739.
[190] A.N. Gorban, I.V. Karlin, *Physica A* 336 (2004) 391–432.
[191] L. Lu, S.B. Pope, *J. Comput. Phys.* 228 (2009) 361–386.
[192] G. Blanquart, H. Pitsch, *Proc. Combust. Inst.* 30 (2005) 2745–2753.